



NTNU – Trondheim
Norwegian University of
Science and Technology

Time-domain simulation of marine structures in irregular seas

Yngve Aarland

Marine Technology

Submission date: June 2014

Supervisor: Jørgen Amdahl, IMT

Norwegian University of Science and Technology
Department of Marine Technology

MASTER THESIS 2014

for

Stud. Techn. Yngve Aarland

Time-domain simulation of marine structures in irregular seas

Tidsplananalyse av marine konstruksjoner i irregulær sjø

For dynamically sensitive marine structures or marine structures subjected to large displacements the extreme response is often determined on the basis of short term time domain simulation of extreme sea states using the environmental contour line method.

A challenge with time-domain analysis is the representation of the sea spectrum. For linear analysis and small displacements it is common to use fast Fourier transform (FFT) of the sea spectrum. In order to avoid repetition of the wave history several thousand of uniformly spaced wave components may be needed. For nonlinear time domain simulations the computational requirements of FFT will become prohibitive. An alternative to FFT is to use a few wave components based on equal area principle. This implies that emphasis is placed on the energy rich parts of the wave spectrum. The accuracy of this method must be demonstrated. Using the computer program USFOS it was shown in a previous master thesis work that this method is quite good for floating structures with eigenperiods far away from the energy rich periods of the wave spectrum, but less accurate for structures with eigenperiods in the range of 4-5 seconds. The results depend also on whether the wave forces are mass dominated or drag dominated. It has been suggested that the accuracy may be improved by increasing the subdivision of the wave spectrum in the vicinity of the structure eigenperiod(s).

In USFOS the built-in algorithm for realisation of irregular seas states is based upon linear wave theory and extrapolation of wave kinematics to the instantaneous sea surface (Wheeler stretching). Improved accuracy is obtained by using 2nd order wave theory for surface elevation Wheeler stretching of linear wave kinematics to the surface, and the user may specify the frequency components of the discretised wave spectrum in the input. Most correct is to base wave kinematics completely on 2nd order theory. In USFOS pre-calculated wave kinematics may be represented on a 3D grid and interpolation to actual structure coordinates. It is of interest to compare these methods with respect to extreme response for dynamically sensitive structures.

The following topics should be addressed in the project work:

1. Familiarize with the MATLAB based open source code program WAFO for analysis of stochastic time processes.
2. Familiarize with the scripting technique for automatic conduction of repetitive simulations with USFOS and post-processing of results (refer <http://www.ivt.ntnu.no/imt/software/usfos:scripting>) .
3. Perform time domain dynamic simulation of tension leg tower for offshore wind turbine, the SWAY concept. Focus is placed on the wave kinematics and structural response of the tower subjected to waves with the turbine in idle position. Simulations shall be carried out with both with constant frequency width and the equal area method. The number of wave components shall be varied.
4. Alternatively, simulations shall be carried out with constant frequency width, but with random frequency within the interval, it is referred to the paper *A comparative study of theoretical models for slow drift sway motions of a marine structure* by Zhao and Faltinsen. Finally, analyses shall also be carried out where the amplitude of each individual wave component shall also be considered a random variable. It is suggested to create a MATLAB program to generate the wave components, which can be read by USFOS.
5. Compare the statistical properties of the simulated histories and assesses the adequacy of using the various methods. It shall be concluded on the required number of wave components to achieve acceptable accuracy.
6. An alternative to direct calculation of wave kinematics is to pre-calculate the kinematics in time and space and to tabulate them in a numerical grid. For a selected method of simulating irregular seas investigate the required resolution of the grid to obtain acceptably accurate results. To the extent time permits perform simulation of the response using 2nd order wave kinematics and compare with the results based on linear theory.
7. Conclusions and recommendations for further work.

Literature studies of specific topics relevant to the thesis work may be included.

The work scope may prove to be larger than initially anticipated. Subject to approval from the supervisors, topics may be deleted from the list above or reduced in extent.

In the thesis the candidate shall present his personal contribution to the resolution of problems within the scope of the thesis work.

Theories and conclusions should be based on mathematical derivations and/or logic reasoning identifying the various steps in the deduction.

The candidate should utilise the existing possibilities for obtaining relevant literature.

Thesis format

The thesis should be organised in a rational manner to give a clear exposition of results, assessments, and conclusions. The text should be brief and to the point, with a clear language. Telegraphic language should be avoided.

The thesis shall contain the following elements: A text defining the scope, preface, list of contents, summary, main body of thesis, conclusions with recommendations for further work, list of symbols and acronyms, references and (optional) appendices. All figures, tables and equations shall be numerated.

The supervisors may require that the candidate, in an early stage of the work, presents a written plan for the completion of the work. The plan should include a budget for the use of computer and laboratory resources which will be charged to the department. Overruns shall be reported to the supervisors.

The original contribution of the candidate and material taken from other sources shall be clearly defined. Work from other sources shall be properly referenced using an acknowledged referencing system.

The report shall be submitted in two copies:

- Signed by the candidate
- The text defining the scope included
- In bound volume(s)
- Drawings and/or computer prints which cannot be bound should be organised in a separate folder.
- The report shall also be submitted in pdf format along with essential input files for computer analysis, spreadsheets, MATLAB files etc in digital format.

Ownership

NTNU has according to the present rules the ownership of the thesis. Any use of the thesis has to be approved by NTNU (or external partner when this applies). The department has the right to use the thesis as if the work was carried out by a NTNU employee, if nothing else has been agreed in advance.

Thesis supervisor

Prof. Jørgen Amdahl

Deadline: February 8th, 2015

Trondheim, September 15th, 2014

Jørgen Amdahl

Preface

This report is the result of my thesis work at the department for Marine technology at the Norwegian University of Science and Technology, NTNU. The Master thesis counts for 30 credits.

The thesis has revolved around response problems and dynamic simulations of irregular sea in the time domain. Focus has been on investigating the adequacy of different methods to realize the sea spectrum in the time domain. The methods that are studied are the Equal Area Principle, constant frequency width with wave frequency randomly selected within the integration interval, and constant frequency width with both randomly selected wave frequency and Rayleigh distributed amplitude. The amount of necessary components to obtain accurate results is also addressed.

I would like to thank my supervisor Professor Jørgen Amdahl for helping me with questions that arose during my thesis work. The thesis work has been done outside the university, and his availability when needed has been essential.

Yngve Aarland

.....

08.02.2015

Summary

For dynamically sensitive marine structures or marine structures subjected to large displacements the extreme response is often determined on the basis of short term time domain simulation of extreme sea states using the environmental contour line method.

A challenge with time-domain analysis is the representation of the sea spectrum. For linear analysis and small displacements it is common to use fast Fourier transform (FFT) for realization of the sea spectrum. In order to avoid repetition of the wave history several thousand of uniformly spaced wave components may be needed. For nonlinear time domain simulations the computational requirements of FFT will become prohibitive. An alternative to FFT is to use fewer wave components based on equal area principle (EAP). This implies that emphasis is placed on the energy rich parts of the wave spectrum. The accuracy of this method must be demonstrated. Using the computer program USFOS it was shown in a previous master thesis work that this method is quite good for floating structures with eigenperiods far away from the energy rich periods of the wave spectrum, but less accurate for structures with eigenperiods in the range of 4-5 seconds. The results depend also on whether the wave forces are mass dominated or drag dominated. It has been suggested that the accuracy may be improved by increasing the subdivision of the wave spectrum in the vicinity of the structure eigenperiod(s).

In USFOS the built-in algorithm for realisation of irregular seas states is based upon linear wave theory and extrapolation of wave kinematics to the instantaneous sea surface (Wheeler stretching). Improved accuracy is obtained by using 2nd order wave theory for surface elevation Wheeler stretching of linear wave kinematics to the surface, and the user may specify the frequency components of the discretised wave spectrum in the input. Most correct is to base wave kinematics completely on 2nd order theory. In USFOS pre-calculated wave kinematics may be represented on a 3D grid and interpolation to actual structure coordinates. It is of interest to compare these methods with respect to extreme response for dynamically sensitive structures.

This thesis investigates the adequacy of using the EAP method, and FFT with increased randomization of wave component frequency (FFTrf and FFTrfa), for realization of the sea spectrum. Additionally, wave kinematics are pre-calculated and given as input for USFOS response analysis. The adequacy of the methods are investigated through dynamic response analysis of the SWAY tower.

A standard FFT realization of the spectrum, with 1000 wave components, have been used to perform a dynamic response analysis in the time domain. This analysis is considered to be a correct solution, and is used as basis for comparing the three other methods.

Analyses have been performed with EAP, FFTrf and FFTrfa methods, using 75,100 and 200 components in separate analyses. The FFTrf and FFTrfa are used to perform additional analyses using 1000 components to further confirm the methods applicability. All analyses have been performed 20 times over using different seeds/phase angles/random parameters for FFT and EAP simulations, and unique wave data input for all FFTrf and FFTrfa analyses. The pre-calculated wave kinematics are based on the use of the FFTrfa method, using 200 components to realize the spectrum.

The wave spectrum used for calculation of wave components and wave kinematics is the JONSWAP spectrum, with parameters: significant wave height $H_s=16.4$, peak period $T_p=17$, and gamma parameter=3.3.

The surface elevation process has been evaluated statistically, and maximums from several result variables have been collected and evaluated. The main focus has been on the goodness of the surface elevation process, and the structural responses.

All simulations are carried out for 1500 seconds, with first 500 seconds not being recorded to the result files. This is done to eliminate any transient response in the beginning of each simulation.

All methods investigated show satisfying results regarding the surface elevation process. The accuracy of the wave profile statistics for the simplified methods when 75 components are used is a little poorer than for simulations based on 100. Best results for the time histories are found for 200 components.

The dynamic responses obtained from simulations using the different methods are also investigated thoroughly. The EAP over predicts the responses for simulations with 75 components, while the the FFTrf and FFTrfa underestimates the responses using 75 components. The best results using the simplified methods of spectrum realization is obtained using the FFTrfa method with 200 components. Both surface elevation process, and load histories resembles the results of the standard FFT method almost identically.

Sammendrag

Dynamisk sensitive strukturer, eller marine farkoster utsatt for store forskyvninger vil ofte være gjenstand for dynamisk tidsplananalyse basert på korttidsstatistisk simuleringer av ekstreme sjøtilstander. En utfordring med tidsplananalyser er realisering av bølgespekteret. En ofte praktisert metode er Fast Fourier transformasjon(FFT) av bølgespekteret. Denne metoden er trygg og gir nøyaktige resultater for struktur som oppfører seg lineært. For struktur med ikke-lineær respons, blir metoden veldig omfattende, og tidkrevende. Metoden krever ofte flere tusen bølgekomponenter for å unngå repetisjon av bølgehistorikk. Og vil kreve høy datakapasitet for utføring av simulering. Det er derfor ønskelig å vurdere godheten av en annen metode, Equal Area Principle(EAP), som en alternativ metode for tidsplananalyser. To variasjoner av FFT metoden er også undersøkt, hvor en regner ut bølgekomponenter fra spekteret ved å bruke en tilfeldig valgt bølgefrequens innenfor komponentens frekvensintervall. Den andre metoden bruker den samme tilfeldig valgte frekvensen i integrasjonsintervallet, og i tillegg betraktes bølgeamplituden som en Rayleigh fordelt variabel. De to sistnevnte metodene er henholdsvis betegnet som FFTrf og FFTrfa heretter.

SWAY tårn for flytende vindkraftturbiner er strukturen som er blitt gjennomført simuleringer på.

Alle metodene er testet med 75,100, 200 bølgekomponenter. I tillegg er FFTr og FFTrf simulering gjort med 1000 komponenter for å ytterligere vurdere metodene. De er deretter sammenlignet opp mot en standard FFT basert analyse med 1000 bølgekomponenter. Den sistnevnte analysen er brukt som sammenligningsgrunnlag for de andre analysene.

Fra analyser er det hentet data hovedsakelig fra bølgehevingsprosessen, og maksimalutslag fra gitte parameter studert i responsanalysen: Cardan kraft, Moment midt på strukturen, Bølgeheving, total bølgelast, aksellerasjon av toppunkt på tårn, sideveis forskyvning av toppunkt på tårn.

Analyser er kjørt i 1500 sekunder for alle simuleringmetoder. De 500 første sekundene er en initieringsfase for å la strukturen utvikle bevegelsesmønster før resultater lagres til fil. Dette gjøres for å unngå transiente effekter i responser lagret i resultatfil.

Alle metoder undersøkt viste tilfredsstillende resultater hva gjelder bølgehevingsprosessen. Dårligst bølgehevingsdata ble funnet for simuleringer kjørt med 75 komponenter. Det var likevel små avvik sammenlignet med hva en kan forvente av simuleringer. Best ut kom metoder kjørt med 100 komponenter eller mer. FFTrfa og FFTrf tilfredstilte teoretiske parametere for normalfordelt bølgeprosess veldig bra.

For dynamisk responsberegning overestimerte EAP metoden resultatene for simuleringer med 75 komponenter, mens FFTrf og FFTrfa underestimerte responsene ved 75 komponenter som beregningsgrunnlag. Best ut kom FFTrf og FFTrfa med bruk av 200 komponenter. Simuleringer med de to sistnevnte metoden fulgte de beregnede data fra standard FFT metode nesten identisk.

Table of Contents

Preface	v
Summary	vi
Sammendrag	viii
Nomenclature	xv
1 Introduction	1
2 Wave theory	2
2.1 Velocity potential theory	2
2.2 Linear wave theory	6
2.3 Irregular sea	8
2.3.1 Wave kinematics for modelling of irregular waves (Wheeler stretching)	8
2.4 The wave spectrum, JONSWAP	10
2.5 Fast Fourier Transformation (FFT), Constant frequency width	12
2.5.1 Constant frequency width, with randomly selected frequency within the frequency interval of integration - (FFT _{rf})	13
2.5.2 Constant frequency width, with randomly selected frequency within the frequency interval of integration, and Rayleigh distributed wave amplitude – (FFT _{rfa})	13
2.6 The Equal Area Principle (EAP)	14
2.7 Grid wave method	15
3 Statistical theory for waves	16
3.1 Gaussian distribution	16
3.2 General definition of moments and central moments	16
3.2.1 Expectation value for a stochastic variable	17
3.2.2 Variance	17
3.2.3 Skewness coefficient	18
3.2.4 Flatness coefficient, kurtosis	18

3.3 Extreme value statistics & distribution of largest maxima.....	19
3.3.1 The Gumbel distribution	19
3.3.2 Probability paper	20
4 The SWAY concept	21
5 Description of software	23
5.1 USFOS	23
5.1.1 USFOS Hydrodynamics	23
5.1.2 USFOS other modelling parameters	25
5.1.3 Scripting of USFOS	25
5.2 MATLAB	26
6 Case Study – Dynamic response analysis in the time-domain of SWAY tower.....	27
6.1 Dynamic equation of motion.....	29
6.2 Damping	30
6.3 Numerical solution of the equation of motion	31
6.4 Dynamic analysis of SWAY tower	33
7 Results and Discussion.....	34
7.1 Verification of results.....	34
7.2 Results of surface elevation process.....	36
7.2.1 Surface elevation process, numerical results.....	36
7.2.2 Gumbel plots of extreme value distribution of wave heights.....	36
7.3 Discussion of surface elevation process results	42
7.3.1 Mean value of surface profile.....	42
7.3.2 Standard deviation/Variance	42
7.3.3 Kurtosis / flatness parameter	42
7.3.4 Skewness parameter	43

7.3.5 Extreme value statistics of surface elevation	43
7.4 Results wave loads from dynamic analysis of SWAY tower.....	45
7.5 Discussion results total wave load	48
7.6 Results dynamic analysis of SWAY tower - response	49
7.6.1 Numeric results from dynamic analysis of SWAY tower - response	49
7.6.2 Gumbel plots for extreme value distributions of response.....	50
7.7 Discussion of Response analysis results SWAY tower	55
7.7.1 Slow-drift motions and sum frequency effects in irregular waves.....	56
8 Conclusion.....	57
9 Recommendation for further work.	58
10 References	59
Appendix	I
A.1 data files/usfos/matlab/bash.....	I
A.2 Complete results	II
A.2.1 Averages collected from all methods	II
A.2.2 Statistics for all time histories ordered for each method.	VI

Figure 1 - Illustration of control volume for mass flow equilibrium	3
Figure 2 - JONSWAP spectrum with $H_s=16.4\text{m}$ $T_p=17\text{s}$ and $\gamma=3.3$	11
Figure 3 - Constant frequency resolution (FFT)(USFOS Hydrodynamics).....	12
Figure 4 -Constant area - varying resolution(EAP)- (USFOS Hydrodynamics)	14
Figure 5 - The SWAY Concept (SWAY A/S)	21
Figure 6 - Damping ratio as function of angular frequency	31
Figure 7 - Gumbel plot FFT1000 - maximum distribution of surface elevation.....	37
Figure 8 - Gumbel plot FFT500 - maximum distribution of surface elevation.....	37
Figure 9 - Gumbel plot EAP75 - maximum distribution of surface elevation.....	37
Figure 10 - Gumbel plot EAP100 - maximum distribution of surface elevation.....	38
Figure 11 - Gumbel plot EAP200 - maximum distribution of surface elevation.....	38
Figure 12 - Gumbel plot FFTrf75 - maximum distribution of surface elevation.....	38
Figure 13 - Gumbel plot FFTrf100 - maximum distribution of surface elevation.....	39
Figure 14 - Gumbel plot FFTrf200 - maximum distribution of surface elevation.....	39
Figure 15 - Gumbel plot FFTrf1000 - maximum distribution of surface elevation.....	39
Figure 16 - Gumbel plot FFTrfa75 - maximum distribution of surface elevation	40
Figure 17 - Gumbel plot FFTrfa100 - maximum distribution of surface elevation	40
Figure 18 - Gumbel plot FFTrfa200 - maximum distribution of surface elevation	40
Figure 19 - Gumbel plot FFTrfa1000 - maximum distribution of surface elevation	41
Figure 20 - Gumbel plot grid200 - maximum distribution of surface elevation	41
Figure 21 - Gumbel plot grid200_1 - maximum distribution of surface elevation	41
Figure 22 - Gumbel plot FFT 1000 and 500, Total waveload.....	46
Figure 23 - Gumbel plot EAP method - Total wave load	46
Figure 24- Total wave load FFTrf method.....	47
Figure 25- Total wave load FFTrfa method	47

Figure 26 - Total wave load Grid wave method 200 components	48
Figure 27 - Gumbel plot Midmoment Mz FFT method	50
Figure 28 - Gumbel plot - Midmoment Mz EAP method	51
Figure 29 - Gumbel plot - Midmoment Mz FFTrf method	51
Figure 30 - Gumbel plot - Midmoment Mz FFTrfa method	52
Figure 31 - Gumbel plot - Midmoment Gridwave method	52
Figure 32 - Gumbel plot - Cardan force FFT method	53
Figure 33 - Gumbel plot Cardan force - EAP method	53
Figure 34 - Gumbel plot - Cardan force FFTrf method	54
Figure 35 - Gumbel plot - Cardan force FFTrfa method.....	54
Figure 36 - Gumbel plot - Cardan force - Gridwave method.....	55

Table 1 – List of methods and variations in wave components	28
Table 2 - Collected statistics of elevation process, all methods.....	36
Table 3 - Theoretical values of statistical parameters, Gaussian sea with $H_s=16.4$ m	42
Table 4- Results from dynamic analysis - Total Wave Load.....	45
Table 5 - Wave load ratio, compared against results from FFT1000 method.....	45
Table 6 - Averages of response from dynamic analysis of sway tower.....	49
Table 7 - Ratios of response results when compared against results from FFT 1000 method.	50

Nomenclature

k = wave number

g = Acceleration of gravity

ϕ = Velocity potential

ζ_a = Wave amplitude

ω = Angular wave frequency

$\zeta(t)$ = sea elevation

N/n = number of wave components

ω_n = angular wave frequency for wave component n

ζ_n = Wave amplitude for component n

k_n = Wave number for component n

ϵ_n = Random angular phase angle for component n , ranging from $0-2\pi$

$S(\omega)$ = Wave spectrum, JONSWAP

ω_p = Top frequency

T_p = the peak period

α = Spectrum parameter

γ = topness parameter

ω = angular wave frequency

σ = JONSWAP spectrum parameter

$\bar{\mu}_x^{(n)}$ - Central moments, statistical parameter

$\mu_x^{(n)}$ - moments, statistical parameter

Abbreviations

EAP – Equal area principle

FFT – Fast fourier transform

FFT_{rf} – Fast Fourier Transform with increased frequency randomization

FFT_{rfa} – Fast Fourier Transform with frequency randomization and Rayleigh distributed amplitude

1 Introduction

For dynamically sensitive marine structures or marine structures subjected to large displacements the extreme response is often determined on the basis of short term time domain simulation of extreme sea states using the environmental contour line method.

A challenge with time-domain analysis is the representation of the sea spectrum. For linear analysis and small displacements it is common to use fast Fourier transform (FFT) of the sea spectrum. In order to avoid repetition of the wave history several thousand of uniformly spaced wave components may be needed. For nonlinear time domain simulations the computational requirements of FFT will become prohibitive. An alternative to FFT is to use a few wave components based on equal area principle(EAP). The accuracy of this method must be demonstrated. In addition the FFT method is approached with two variations. One makes use of a randomly selected wave frequency selected within the components interval of integration. The other makes use of the above mentioned random frequency, and treats the wave amplitude as a Rayleigh distributed random variable. The three methods are tested for dynamic response analysis in the time domain, using a varying amount of components for the each method. In addition to the adequacy of the investigated methods, the necessary amount of wave components is also addressed. For possible reduction of analysis time, wave kinematics are calculated using the FFT method with random frequency and amplitude. The data are tabulated grid with kinematic data in time space. The grid wave is used for input to calculate the response.

Thesis outline

The purpose of this thesis is to investigate the adequacy of the proposed methods to simulate irregular sea. A dynamic response analysis is to be performed using these methods to simulate irregular sea. The analysis is carried out using USFOS. After conferring with my supervisor, Professor Jørgen Amdahl, it was concluded that only a dynamic analysis using these methods should be carried out.

Chapter 2 presents theoretic background for wave theories used throughout this thesis work.

Chapter 3 presents statistical theory used for evaluation of stochastic variables

Chapter 4 Describes the SWAY floating wind turbine

Chapter 5 Describes the USFOS software used, as well as MATLAB and the use scripting for efficient running of simulations.

Chapter 6 presents the studies and methods/theory regarding the dynamic analysis of the sway structure.

Chapter 7 Presentation and discussion of results found from the dynamic analyses.

Chapter 8 Conclusion

2 Wave theory

This chapter is dedicated to briefly present wave theory that is used throughout the thesis work.

The goodness of a dynamic response analysis for a marine structure exposed to wave loads is dependent on how well the waves are modelled. Linear wave theory is widely applied, and is proven accurate for problems involving small structural displacements. When displacements become large, we are in need of high accuracy in our analysis, and 2nd order wave theory must be applied to get the correct interaction between wave and response. This subchapter will present the most relevant theories for establishing accurate wave kinematics.

2.1 Velocity potential theory

To describe the sea water analytically, we must assume some physical properties for the behaviour of the fluid. *The water is assumed incompressible and invicid. The fluid motion is irrotational*[1]. If these properties are valid for the fluid, we can describe the fluid velocity vector \mathbf{V} , in time and space, by a velocity potential ϕ .

$$\mathbf{V} = \nabla\phi \equiv \mathbf{i} \frac{\partial\phi}{\partial x} + \mathbf{j} \frac{\partial\phi}{\partial y} + \mathbf{k} \frac{\partial\phi}{\partial z} = (u, v, w) \quad (2.1)$$

Where \mathbf{i} , \mathbf{j} and \mathbf{k} are unit vectors along the Cartesian coordinate axes, x, y and z respectively. We have assumed that the fluid is incompressible, and thus a constant density for the fluid. If we set up an equilibrium equation for the flow of mass inside a control volume, for an incompressible fluid, we end up with the continuity equation:

If we have a cube with sides dx , dy and dz , where fluid, with density ρ , flows through the cube with velocity u , the instantaneous flow of mass per unit time through a flat square, $dy \cdot dz$, becomes for flow in the x -direction:

$$\dot{m}_x = \rho u dy dz$$

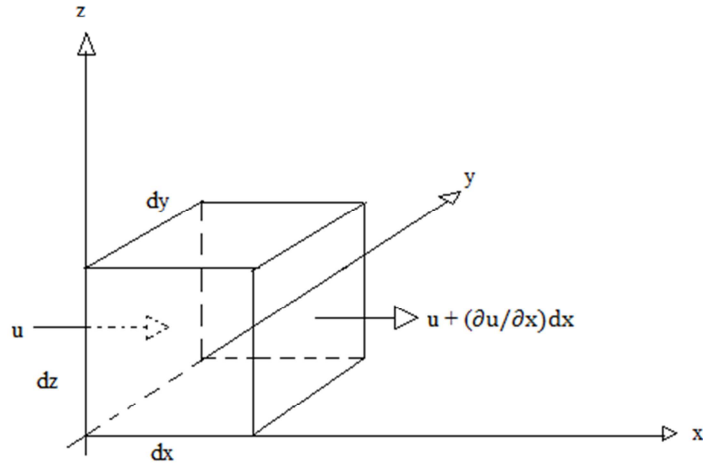


Figure 1 - Illustration of control volume for mass flow equilibrium

Mass equilibrium, the change in mass because of change in density must be equal to the difference between incoming and outgoing flow of mass:

$$\frac{\partial \rho}{\partial t} dx dy dz = - \left[\frac{\partial(\rho u)}{\partial x} + \frac{\partial(\rho v)}{\partial y} + \frac{\partial(\rho w)}{\partial z} \right] dx dy dz \quad (2.2)$$

Equation (2.xx) above results in the continuity equation,

$$\frac{\partial \rho}{\partial t} + \frac{\partial(\rho u)}{\partial x} + \frac{\partial(\rho v)}{\partial y} + \frac{\partial(\rho w)}{\partial z} = 0 \quad (2.3)$$

which for an incompressible fluid will have constant density, and thus reduces to,

$$\frac{\partial u}{\partial x} + \frac{\partial v}{\partial y} + \frac{\partial w}{\partial z} = 0 = \nabla \cdot \mathbf{V} \quad (2.4)$$

It then follows that for an irrotational, incompressible fluid, we can write:

$$\begin{aligned}\mathbf{V} &= \nabla\phi \\ \nabla \mathbf{V} &= \mathbf{0} \\ \nabla^2 \phi &= 0\end{aligned}\tag{2.5}$$

So for irrotational flow of an incompressible fluid, we can express the flow by its velocity potential explicitly.

Excerpts from “Marin Teknikk 3 – Hydrodynamikk” – B. Pettersen, 2007, and “Sea loads on ships and offshore structures” – O.M. Faltinsen, 1990, regarding velocity potential theory and waves are given below.

In addition to satisfying the Laplace equation, the velocity potential describing the waves needs to fulfill a set of conditions:

- Equation of continuity(Laplace)
- Normal velocity against seabed shall be equal to zero when we have finite water depth
- Bernoullis equation must be valid on sea surface(Dynamic condition)
- The kinematic conditions at sea surface must be satisfied

Below is a description of how these boundary conditions are applied for two dimensional waves. Vertical depth in z-direction is defined so that $z = 0$ **at the surface**, and $z = -d$ **at seabed**.

The Laplace equation becomes:

$$\frac{\partial^2 \phi}{\partial x^2} + \frac{\partial^2 \phi}{\partial y^2} + \frac{\partial^2 \phi}{\partial z^2} = 0\tag{2.6}$$

Seabed boundary condition:

$$\frac{\partial \phi}{\partial z} = 0, \quad \text{for } z = -d \text{ (at seabed)}\tag{2.7}$$

The vertical velocity through the sea floor must be zero.

Dynamic free surface condition:

The Bernoulli equation must be satisfied at the sea surface, meaning that the water pressure at the sea surface must be equal to the atmospheric pressure.

The resulting equation becomes

$$g\zeta + \frac{\partial\phi}{\partial t} + \frac{1}{2}\left(\left(\frac{\partial\phi}{\partial x}\right)^2 + \left(\frac{\partial\phi}{\partial y}\right)^2 + \left(\frac{\partial\phi}{\partial z}\right)^2\right) = 0, \quad z = \zeta(x, y, t) \quad (2.8)$$

The bold terms on the left side of the equation is a nonlinear contribution to the description of the sea surface pressure. The problem is often simplified to only consist of the linear contributions. This is a valid approach in several problems, but for wave-response problems where displacements and/or waves become large, we must consider the non-linear interactions as well.

Kinematic boundary condition:

A fluid particle on the free-surface is assumed to stay on the free-surface [Faltinsen].

$$z = \zeta(x, y, t)$$

$$\frac{\partial\zeta}{\partial t} + \frac{\partial\phi}{\partial x} \frac{\partial\zeta}{\partial x} + \frac{\partial\phi}{\partial y} \frac{\partial\zeta}{\partial y} = \frac{\partial\phi}{\partial z} \quad (2.9)$$

The bold terms in the equation are nonlinear contributions. The linear terms express that the time derivative of the elevation is equal to the vertical velocity of the surface fluid particle, at $z = \zeta(x, y, t)$

Combining the kinematic and dynamic boundary conditions will eliminate ζ from the equations, and we get:

$$-\frac{\partial^2\phi}{\partial t^2} - g \frac{\partial\phi}{\partial z} - \left(\frac{\partial}{\partial t} + \frac{1}{2}\nabla\phi \cdot \nabla\right) |\nabla\phi|^2 = 0, \quad z = \zeta(x, y, t) \quad (2.10)$$

2.2 Linear wave theory

For this thesis, waves are modelled using linear wave theory, also called Airy theory. The basis for the theory is given by reducing the above mentioned equations to their linear forms. This theory is valid when wave amplitude is small relative to the wavelength and dimension of the body subjected to waves. When the nonlinear terms of the boundary conditions are neglected, the problem becomes a lot easier to solve. The boundary conditions for the linear problem are [Faltinsen]:

$$\begin{aligned}
 \frac{\partial \zeta}{\partial t} &= \frac{\partial \phi}{\partial z} \quad \text{on } z=0, && \text{Kinematic condition} \\
 g\zeta + \frac{\partial \phi}{\partial t} &= 0 \quad \text{on } z=0, && \text{Dynamic condition} \\
 \frac{\partial \phi}{\partial z} &= 0, \quad \text{for } z = -d \text{ (at seabed)} && \text{Sea bottom condition} \\
 \frac{\partial^2 \phi}{\partial x^2} + \frac{\partial^2 \phi}{\partial y^2} + \frac{\partial^2 \phi}{\partial z^2} &= 0 && \text{The Laplace equation}
 \end{aligned} \tag{2.11}$$

Water depth considered to be deep, $\frac{d}{\lambda} > 0.5$. Wavelengths are ranging from 100+m to 10m. The JONSWAP wave spectrum is used for calculation of the wave components, and the wavelength for the most energy rich waves are between 50, and 75 m with significant waveheight 16.4 meters. The validity of linear theory seems fair, when comparing the dimension the structure (sway tower), which has a cylinder shape with diameter less than 9.2 meters for all wetted surfaces.

In the following section the velocity potential problem for linear waves in finite and deep waters is derived using the boundary conditions and assumptions given above.

From the dynamic condition, we know that the velocity potential must be of the form:

$$\phi = f(z) \sin(kx - \omega t) \tag{2.12}$$

When we introduce the demand that the velocity potential must satisfy the Laplace equation, we must solve the differential equation that is produced. The solution which satisfies the Laplace equation is:

$$\phi = (Ae^{kz} + Be^{-kz}) \sin(kx - \omega t) \tag{2.13}$$

The sea bottom boundary condition tells us that

$$\frac{\partial \phi}{\partial z} = 0 \text{ at } z = -d \tag{2.14}$$

The resulting equation becomes

$$(kAe^{-kd} - kB e^{kd}) \sin(kx - \omega t) = 0 \tag{2.15}$$

$$Ae^{-kd} = Be^{kd} \quad (2.16)$$

The above equation is solved to find the constants A and B, and when introducing the definition of hyperbolic functions, the velocity potential now looks like this.

$$\phi = C \cosh(k(d+z)) \sin(kx - \omega t) \quad (2.17)$$

With C being an unknown constant.

The dynamic condition tells us that C must be,

$$C = \frac{g\zeta_A}{\omega \cosh(kh)} \quad (2.18)$$

And we end up with the velocity potential for waves expressed like this [11]:

$$\phi = \frac{g\zeta_A \cosh(k(d+z))}{\omega \cosh(kh)} \sin(kx - \omega t) \quad (2.19)$$

As the water depth increases, the hyperbolic terms in the equation above reduces to e^{kz} , and for deep water waves we get:

$$\phi = \frac{g\zeta_A}{\omega} e^{kz} \sin(kx - \omega t) \quad (2.20)$$

The dispersion relation relates wave frequency and wavenumber k, for finite water depths it is given as:

$$\omega^2 = kg \tanh(kd) \quad (2.21)$$

We use the equations for deep water waves when $d > \lambda/2$ [11].

2.3 Irregular sea

The waves used for analyses have been modelled as long crested waves propagating in the same direction. For these linear 2-D wave components, the principle of superpositioning is valid. With this assumption we can model an irregular sea as a sum of several regular harmonic wave components, where each wave component are assigned random phase angles. The two-dimensional sea elevation in time and space is then described as:

$$\zeta(\mathbf{t}) = \sum_{n=1}^N \zeta_n \cos(\omega_n t - \mathbf{k}_n \mathbf{x} + \epsilon_n) \quad (2.22)$$

Where:

N = number of wave components

ω_n = angular wave frequency for wave component n

ζ_n = Wave amplitude for component n

\mathbf{k}_n = Wave number for component n

ϵ_n = Random angular phase angle for component n , ranging from $0-2\pi$

The individual wave components and amplitudes used when modelling irregular sea may come from various means. Either they come from observational data, from statistical/empirical studies, or from calculations based on internationally accepted conventions, such as a standardized wave spectrum/wave energy density distribution. The latter is the basis for the studies and analyses done in this work.

2.3.1 Wave kinematics for modelling of irregular waves (Wheeler stretching)

The work and analyses in this thesis is based on linear wave theory. The most common way of calculating wave kinematics for linear irregular sea is proposed by Wheeler[12]. When linear potential flow theory is used to calculate wave kinematics, the kinematics were shown to be overestimated at the surface. A correction, introduced by Wheeler, was to stretch the kinematics calculated at the mean surface $z=0$ up to the instantaneous sea surface. This was supported by measurements of the real surface kinematics. The correction of the vertical coordinate when calculating wave kinematics from the velocity potential is given in equation (2.23). The corrected vertical coordinate z' is switched with z in equation

$$z' = \frac{(z+\eta)}{(d+z)} \cdot d \quad (2.23)$$

This technique is used for the calculations done when creating input for simulations using a grid wave. The grid wave method is described in chapter 2.7 of the report.

When linear theory described in chapter 2.1 and 2.2 is used to calculate wave kinematics, the equations for fluid particle velocity (2.24) and acceleration(2.25) in horizontal x-direction becomes:

$$u_n(x, z, t) = \frac{k_n g \zeta_n \cosh(k_n(d+z))}{\omega \cosh(k_n d)} \cos(k_n x - \omega_n t + \epsilon_n) \quad (2.24)$$

$$a_n(x, z, t) = k_n g \zeta_n \frac{\cosh(k_n(d+z))}{\cosh(k_n d)} \sin(k_n x - \omega_n t + \epsilon_n) \quad (2.25)$$

Where:

d= water depth

k_n =wave number

z= vertical position, use z' in eq(2.23) for wheeler stretching

x= horizontal position

g=gravitational acceleration

ϵ_n = phase angle

ω_n = wave frequency

ζ_n =wave amplitude

As linear theory is applied, the principle of superpositioning is valid. The contributions of wave kinematics for each wave component is then summed up to form the wave kinematics for the sea surface at position (x,z) and in time t. Equations 2.26 and 2.27 describes the principle, where N is the total amount of wave components.

$$u(x, z, t) = \sum_{n=1}^N u_n(x, z, t) \quad (2.26)$$

$$a(x, z, t) = \sum_{n=1}^N a_n(x, z, t) \quad (2.27)$$

2.4 The wave spectrum, JONSWAP

An important quantity when doing a stochastic response analysis is the wave spectrum characterizing the sea elevation process [2]. There are several different standardized wave spectrums available, such as the Pierson-Moskowitz spectrum, Torsethaugen spectrum and JONSWAP. These three are common to use for Nordic sea conditions. The spectrum selected to be used in this work is the JONSWAP spectrum. This spectrum has been used in previous similar studies, and comparison studies of results obtained in this study might benefit from using similar data as basis.

The JONSWAP wave spectrum is formulated like this:

$$S(\omega) = \alpha g^2 (2\pi)^{-4} \omega^{-5} \exp\left(-\frac{5}{4} \left(\frac{\omega}{\omega_p}\right)^{-4}\right) \gamma \exp\left\{-\frac{\left(\frac{\omega}{\omega_p}-1\right)^2}{2\sigma^2}\right\} \quad (2.24)$$

Where:

ω_p = Top frequency = $\frac{2\pi}{T_p}$, Where T_p is the peak period

α = Spectrum parameter

γ = topness parameter

ω = angular wave frequency

σ = is another parameter that tells us about the shape of the spectrum in the most energy dense part of the wave spectrum.

$$\sigma = \begin{cases} \sigma_a & \text{for } \omega \leq \omega_p \\ \sigma_b & \text{for } \omega > \omega_p \end{cases}$$

The wave spectrum is the quantity from which the harmonic wave amplitudes are calculated from. The relation between the wave spectrum and the wave amplitude, and thus also the sea elevation process is described in equation 2.25. Figure 2 shows the JONSWAP spectrum with parameters used in this work.

$$\zeta_n = \sqrt{2 \int_{\omega-lo}^{\omega-up} S(\omega_n) d\omega} \quad (2.25)$$

Where:

ζ_n = Wave amplitude for wave component n

ω_n = Angular wave frequency for wave component n

$\omega - lo/up$ = Upper and lower limits for the frequency band/interval from which the wave component is calculated from

$S(\omega_n)$ = Corresponding spectral value for wave frequency n.

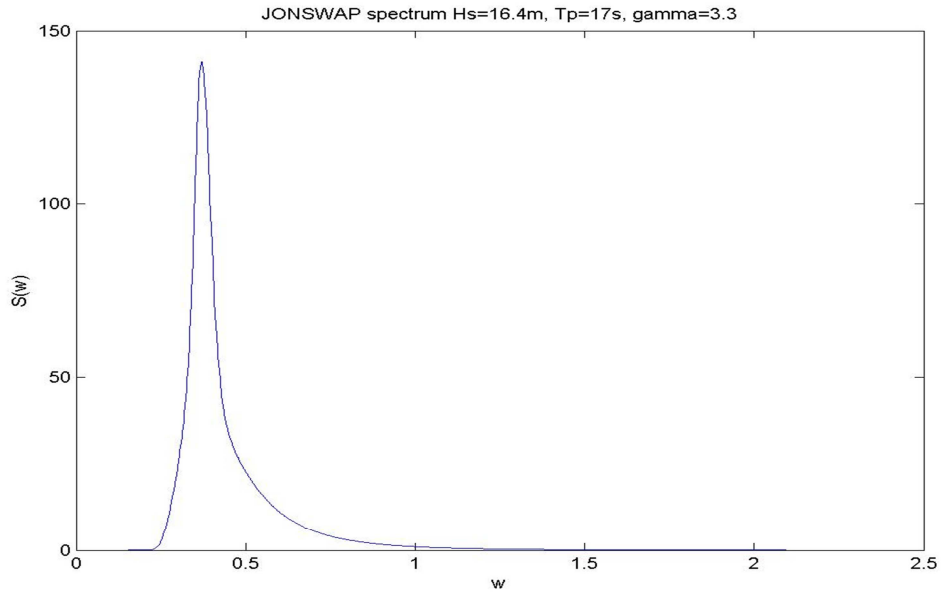


Figure 2 - JONSWAP spectrum with $H_s=16.4\text{m}$ $T_p=17\text{s}$ and $\gamma=3.3$

The integral formulation in equation (2.25) is calculated numerically in this work, and two methods of formulating this integration are studied. The varying frequency width method, also called the equal area principle (EAP), and the constant frequency with or Fast Fourier Transform (FFT). The latter method is also investigated with certain adjustments regarding randomization of parameters. The concepts are described in the following sections of this chapter.

2.5 Fast Fourier Transformation (FFT), Constant frequency width

Fast Fourier Transformation of the wave spectrum is a common way to approach dynamic response analysis in the time domain for marine structures. The method has been proven accurate and good for linear response problems. For accurate results, this approach can require several thousand individual wave components, using constant frequency width. The amount of necessary wave components depends on the duration of the analysis. For non-linear problems this method becomes time-consuming due the computational requirements. The minimum recommended amount of wave components needed to avoid repetition of wave histories is so that $\Delta\omega \leq \pi/T$ [10], where $\Delta\omega$ is the frequency range where the spectrum contains energy, and T is the duration of the analysis in seconds. The concept of constant frequency width, for N wave components, is formulated mathematically below. This method of integration will produce wave components with variable amplitudes, where the largest amplitudes are found when calculating components from the most energy rich parts of the spectrum.

$$\Delta\omega = \frac{\omega_{n-up} - \omega_{n-lo}}{N} = \text{constant} \tag{2.26}$$

A figure explaining the integration concept in use, is given below

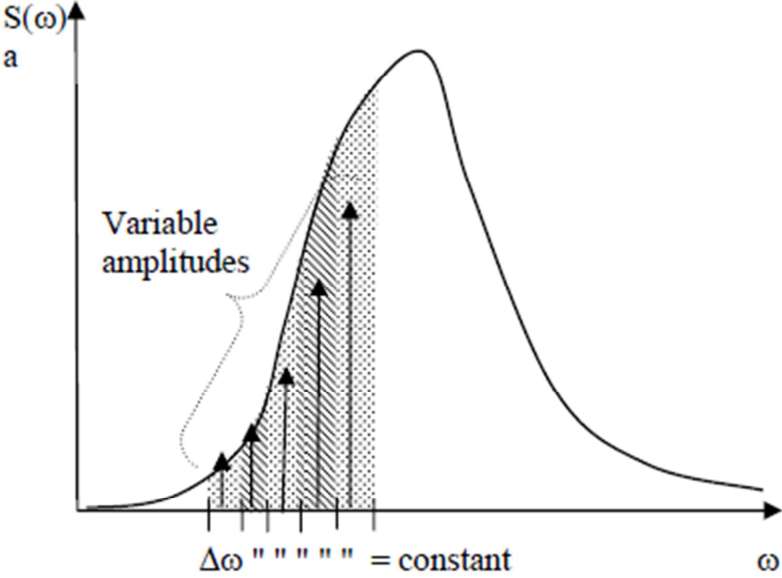


Figure 3 - Constant frequency resolution (FFT)(USFOS Hydrodynamics)

When using the standard FFT method, the wave component amplitude are calculated like this:

$$\zeta_n = \sqrt{2 S(\omega_n) \Delta\omega} \quad (2.27)$$

Where $\Delta\omega$ is the frequency bandwidth found from (2.6). ω_n is selected as the middle frequency in the interval range for the given component: $\omega_n = \frac{\omega_{lo-n} + \omega_{hi-n}}{2}$, where ω_{lo-n} and ω_{hi-n} is the lower and upper limits of the frequency interval. The phase angle for the component is treated as a random variable, uniformly distributed between 0 and 2π .

2.5.1 Constant frequency width, with randomly selected frequency within the frequency interval of integration - (FFTrf)

For the standard FFT method with constant frequency width applied in USFOS, the wave components are calculated using a middle frequency. When varying the seed in USFOS for any given analysis/time series, only the phase angle is treated as a random variable. A suggestion to select a random wave frequency from within the frequency interval for the component will give more randomness to the simulated sea surface. Studies done by R. Zhao and O. M. Faltinsen, has shown that the elevation process will not repeat as fast as for standard FFT, when using a randomly selected frequency in the calculation interval. Thus one can perform longer analyses using fewer components. USFOS cannot do this with built in commands, so these wave components are calculated using MATLAB, and then used as input for USFOS when performing the analysis. Refer to the paper written by R. Zhao and O. M. Faltinsen; *A comparative study of theoretical models for slow-drift sway motion of a marine structure*, for details regarding the concept[8].

The frequency of each wave component is treated as a uniformly distributed variable, within the frequency interval limits. Calculation of the component frequency becomes:

$\omega_n = \omega_{lo-n} + (\omega_{hi-n} \cdot \mathbf{u})$, with \mathbf{u} being a random number between 0 and 1. The phase is still selected randomly as for the standard FFT.

2.5.2 Constant frequency width, with randomly selected frequency within the frequency interval of integration, and Rayleigh distributed wave amplitude – (FFTrfa)

In addition to selecting random wave frequency from within the integration interval, the wave amplitude is treated as random variable also. This way of determining wave component amplitudes is the recommended practice, given by DNV- RP-C205 [20], for time domain simulation of irregular seas.

2.6 The Equal Area Principle (EAP)

EAP method suggests a different approach for calculating the sea surface elevation. Where the FFT method makes use of a fixed frequency width for calculating the spectral density integral, the EAP method demands constant energy amplitude for the integrated area, and thus equal wave amplitudes. This is done by adjusting the integration limits so that it produces an equal area/amount of energy for each component. Equation (2.28) explains the concept. And illustration of the integration procedure is shown in figure 4.

$$\zeta_n = \sqrt{2 \int_{\omega-lo,n}^{\omega-up,n} S(\omega) d\omega} = \text{constant} = \sqrt{\frac{2 \int_{\omega-lo}^{\omega-up} S(\omega_n) d\omega}{N}} \quad (2.28)$$

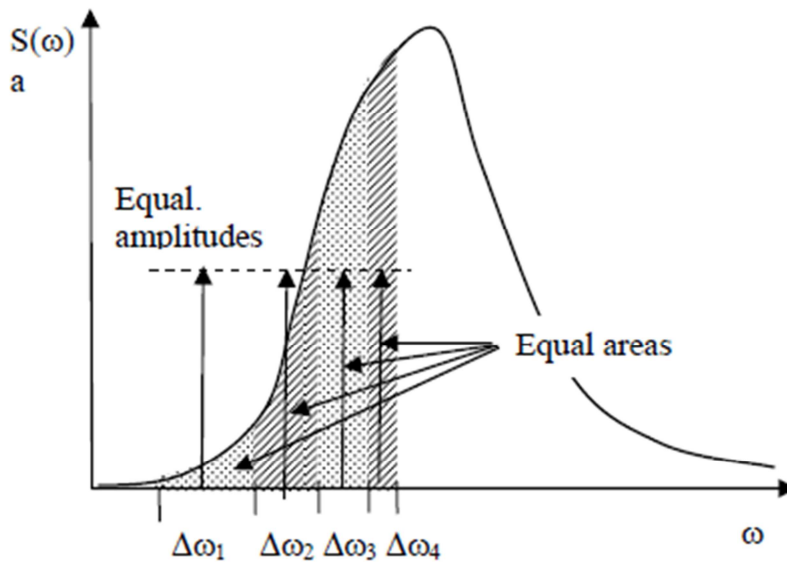


Figure 4 -Constant area - varying resolution(EAP)- (USFOS Hydrodynamics)

The equal area principle does not demand the same great number of wave components as with the FFT method. This is due to the fact that the EAP results in repeating wave histories only after very long time [3][4]. This method only calculates waves with random phase angles, and same amplitude. This idealization does not support the actual realization of the sea surface. For best realization compared to real sea surface elevation, both wave amplitudes and phase angle should be random, and thus Gaussian distributed.

2.7 Grid wave method

A suggested alternative to direct calculation of wave kinematics in USFOS, is to pre-calculate the kinematics in time and space, and tabulate the data in a numerical grid. This method is supported by USFOS, and input is given as a data file.

The wave kinematics are calculated using linear wave theory, and linear velocity potential flow theory described in chapter 2.1 and 2.2. When calculating velocity and acceleration, wheeler stretching of the sea surface is used to correct for over estimation of the wave kinematics at the sea surface. The principle of Wheeler stretching is described in chapter 2.3.

The data input is stored in a gridwave file, and contains data groups for surface elevation, particle velocity and acceleration for a desired amount of coordinates/nodes in space, and for each desired time step. The description of how this file is constructed is given in USFOS theory manual for user input [16].

3 Statistical theory for waves

The main focus in this thesis is to find effective but sufficiently accurate ways to simulate irregular waves in the time domain. Irregular sea is usually described statistically. To investigate the goodness of the simplified ways of modelling the waves, one needs to perform statistical evaluations of the output from the simulations performed. This chapter will present theory used to describe random stochastic processes.

3.1 Gaussian distribution

The surface elevation process is assumed to be a stationary, normal distributed stochastic process [5]. It is assumed that the variation of the statistical characteristics of the process is much slower than the variations of the sea surface [2]. So the assumption that the surface elevation process is stationary is valid within a limited time period, typically less than 3 hours. The simulations done in this thesis is within this specified time period range. When these assumptions are applied to the surface elevation, the conditions for a Gaussian distributed variable are satisfied. The probability density function for the Gaussian distribution is given below:

$$f_{\zeta}(\zeta) = \frac{1}{\sigma_{\zeta}\sqrt{2\pi}} e^{-\frac{1}{2}\left(\frac{\zeta-\mu_{\zeta}}{\sigma_{\zeta}}\right)^2} \quad (3.1)$$

With

ζ = Stochastic variable for surface elevation

σ_{ζ} = Standard deviation for the surface elevation

μ_{ζ} = Expected/mean value for the surface elevation

3.2 General definition of moments and central moments

The moments and central moments describe the properties of a stochastic process. These quantities are a very important tool when investigating such processes. Below is an excerpt from Bernt Leira - *Probabilistic Modelling and Estimation*, regarding description of a stochastic variable by its moments.

For a complete description of a stochastic variable by means of its moments, we must in general include an infinite number of moments. In practice, this is impossible, and the only methods available for description of a variable by its moments are based on inclusion only of moments up to a certain order. This implies that we no longer have a complete description, but an approximate description. The fewer moments, the more rough the description will be. Describing a stochastic variable by only its second order moments, is generally a rough description. For samples of small size, the accuracy of moments above 2nd order will be more uncertain. However, if the variable in question is normally distributed (Gaussian), the second order moments give a complete description of the variable[6]

For a continuous stochastic variable, the moments and central moments are defined as :

$$\text{Moments : } \mu_x^{(n)} = \int_{-\infty}^{\infty} x^n f_x(x) dx \quad (3.2)$$

$$\text{Central moments: } \bar{\mu}_x^{(n)} = \int_{-\infty}^{\infty} (x - \mu_x)^n f_x(x) dx \quad (3.3)$$

Where:

x = stochastic variable

$f_x(x)$ = probability density function

3.2.1 Expectation value for a stochastic variable

The expected value is defined as the first order moment for a stochastic variable. The value represents the “center of gravity” for the distribution [6]. The Gaussian sea elevation process has theoretic expectation value $E[X] = 0$.

$$\mu_x^{(1)} = E[X] = \int_{-\infty}^{\infty} x f_x(x) dx \quad (3.4)$$

For a sample, the expected mean value is calculated like this:

$$E[X] = \frac{1}{N} \sum_{n=1}^N x_n \quad (3.5)$$

3.2.2 Variance

The variance for a stochastic variable is defined as the 2nd order central moment. It describes the spreading of the distribution/sample values. The variance is connected to the standard deviation for a sample, as the standard deviation is defined as the square root of the variance. For a continuous stochastic variable:

$$\bar{\mu}_x^{(2)} = \int_{-\infty}^{\infty} (x - \mu_x)^2 f_x(x) dx = \sigma_x^2 \quad (3.6)$$

For a sample:

$$VAR[X] = \frac{1}{N-1} \sum_{n=1}^N (x_n - E[X])^2 \quad (3.7)$$

3.2.3 Skewness coefficient

The skewness of a stochastic variable is defined as the third moment. It describes the grade of symmetry for a distribution around its mean. Positive skewness coefficient, γ_1 , means that the distribution has higher density of extreme values. If skewness coefficient is zero, the distribution is symmetric. The normal distribution has skewness coefficient equal to zero.

For a continuous variable:

$$\gamma_1 = \frac{\bar{\mu}_x^{(3)}}{(\bar{\mu}_x^{(2)})^{\frac{3}{2}}} = \frac{\bar{\mu}_x^{(3)}}{\sigma_x^3} \quad (3.8)$$

For a sample:

$$\gamma_1 = \frac{\frac{1}{N} \sum_{n=1}^N (x_n - E[X])^3}{VAR[X]^{3/2}} \quad (3.9)$$

3.2.4 Flatness coefficient, kurtosis

The flatness coefficient, γ_2 , considered as the 4th order moment for a stochastic variable, and tells us something about the peakedness of the distribution. For a normal distribution this coefficient is equal to 3. Higher values suggest a steeper shaped distribution around its mean, while lower values than 3 suggest a more flat shaped distribution.

$$\gamma_2 = \frac{\bar{\mu}_x^{(4)}}{(\bar{\mu}_x^{(2)})^2} = \frac{\bar{\mu}_x^{(4)}}{\sigma_x^4} \quad (3.10)$$

For a sample:

$$\gamma_2 = \frac{\frac{1}{N} \sum_{n=1}^N (x_n - E[X])^4}{VAR[X]^2} \quad (3.11)$$

3.3 Extreme value statistics & distribution of largest maxima

When evaluating the results from a time-domain analysis, and also stochastic processes in general, we are often interested in the distribution of maximum values of output from the analysis. Samples of peak values are collected from the analyses and the sample distributions are evaluated. The probabilistic models used to evaluate the distributions are presented below.

Following assumptions are applied when choosing probability models [6][7]:

- All wave peaks are identically Rayleigh-distributed
- All maxima are statistically independent and identically distributed
- Wave elevation process is stationary for the 3-hour duration of the process
- Wave elevation process is Gaussian distributed

3.3.1 The Gumbel distribution

The irregular sea modelled in this work is Gaussian distributed. The distribution of peaks for a Gaussian process is Rayleigh distributed. For the Rayleigh distribution, together with Normal, Log-normal, Exponential, Weibull and Rice distribution, the upper tail behavior of the distributions will converge towards the Gumbel extreme value distribution [6]. Cumulative and density distribution functions are respectively defined as:

$$F_y(y) = \exp\{-\exp\{-\alpha(y - u)\}\} \quad (3.12)$$

$$f_y(y) = \alpha \exp\{-\alpha(y - u) - \exp\{-\alpha(y - u)\}\} \quad (3.13)$$

Where:

y = Maxima from sample

α = Gumbel parameter

u = Gumbel parameter

3.3.2 Probability paper

The concept of using probability paper is motivated by making it easier to examine if a probability model, is a good fit for the sample distribution. The Gumbel probability paper is created by linearization of the cumulative distribution function. If X denotes the horizontal axis, and $Y = -\ln(-\ln(F_y(y)))$ as the vertical axis, the Gumbel distribution function will result in a straight line.

Testing a probability model usually requires relatively objective tools to be able to reject or approve the model. This can require a great deal of computations. In an early stage of analysis we are frequently more interested in assessing whether a proposed type of model seems to be reasonable on a more visual basis. Plotting on a probability paper is a subjective method for verification of a selected distribution, as the criteria for rejecting the model is based on visual observations of how much the samples deviate from the straight line, and decided by the observer [6].

The linearized Gumbel distribution that is plotted for a probability paper:

$$Y = -\ln\left(-\ln\left(F_y(y)\right)\right) = \alpha(y - u) = \alpha y - b \quad (3.14)$$

Where:

α = slope

b = intersection of y-axis

The equation to calculate the cumulative probability for a given extreme value sample is given as:

$$F_i = \frac{i}{1+N} \quad (3.15)$$

Where:

i = denotes the cumulative amount of sample values, $i = [1, N]$

N = total number of sample values

4 The SWAY concept

The patented SWAY system is based on a floating tower which extends far below the water surface. The tower consists of a floating pole with ballast in the lower end, similar to a floating bottle. The tower, which is filled with ballast, has its center of gravity located far below the center of buoyancy of the tower. This gives the tower sufficient stability to resist the large loads produced by the wind turbine mounted on top of it. The floating tower is either anchored with a universal joint (articulation) directly to a single seabed anchor in as little as 55m water depth, or at larger water depths, by using a single pipe between the tower and the single anchor.[9]

The turbine can be mounted both upwind and downwind on the tower. However, when the wind hits the rotor the tower is tilting some 5-8 degrees. By tilting the rotor the opposite way which is made possible by placing the rotor downwind of the tower, the rotor is kept perfectly aligned with the wind when the tower tilts. When the wind changes direction, the entire tower turns around a subsea swivel at the bottom of the tower by individually pitching the blades to create the necessary yawing moment (i.e. no yaw motors are required).[9]

By eliminating the need of a yaw motor, and having the whole foundation tower rotate to align with the wind direction, the structure can be reinforced with a tension rod system. This solution of structural reinforcement results in the tower being able to carry a much larger turbine than other structures of similar steel weight. The SWAY system is designed to operate on water depths ranging from 60m to 300m+. The tower is designed to carry commercially available wind turbines in the 2,5-12MW class.



Figure 5 - The SWAY Concept (SWAY A/S)

In this work the SWAY tower without a turbine is modelled and analyzed. In the turbines place, a fixed horizontal node load is placed, as well as a nodal mass. The stripped down model is justified as the dynamic effects of a rotating turbine might have on the response has not been in focus.

The main dimensions of the tower are given below:

Tower height: 194 m (94m above sea surface, 100 m submerged)

Mooring line: 50m(water depth: 150m)

Tower diameter: From mooring swivel to 14m below surface level: 7.3m-9.2m

Tower diameter: From 14m below surface to 15 m above surface: 4-5m

The details of the analysis model can be found in the digital attachment to the report

5 Description of software

The analyses done in this thesis have been done by extensive use of existing computer tools. USFOS has been the software used to execute the dynamic simulations in the time domain, using both built in commands and input generated by external calculations done in MATLAB. MATLAB has also been used for post processing of results.

5.1 USFOS

The software used to run the analyses throughout the thesis work is USFOS. USFOS is the leading engineering software for collapse analyses and accidental load analyses for fixed offshore structures. The program is also efficient for floating structures. This chapter will present some of the theory the software is based on, with focus on the theories used for dynamic response analysis in the time-domain, and simulation of irregular sea.

The software makes use of input data given in one, or up to three separate files of type .fem. A common approach is to separate data strictly dedicated to the model of the structure, like geometric and material properties, in one model-file. The commands related to execution of the analysis, such as loading and storage of results, in one control-file.

The USFOS software consists of several separate modules developed for specific tasks. The most important ones is the analysis module. This is a terminal based program designed to run in the unix-environment. A graphical user interface version (Xact/USFOS GUI) has been created as well, which can operate in a Windows environment. This module does all computations and generates analysis data. Other modules used in this thesis work are Dynmax and Dynres. These are important tools for post processing of analysis data from time-domain simulations.

5.1.1 USFOS Hydrodynamics

There are several built in theories and possibilities for calculating environmental and hydrodynamic loads in USFOS. The wave theories available in USFOS are: Linear (Airy) theory for finite, shallow and infinite water depth, Stokes 5th order wave theory, and Dean's Stream function theory. Built in wave spectrums JONSWAP and Pierson-Moskovits are available for generating wave components when simulating irregular sea, with user configured spectrum parameters. Another option is to use user defined spectrum, which allows for user to give externally calculated wave components as input.

When using built in spectrums, one has the option of selecting which method to calculate wave components. One can either use the FFT formulation, or EAP. Linear wave theory is used when calculating the components, and the sea surface is created by super positioning of these. A phase angle is assigned to each component, and when running several time series, the randomization of these phase angles are controlled by the user selected seed number. A more complete description on how components are calculated in USFOS with the two different methods is found in chapter 2.5 and 2.6.

When the components are calculated and the time domain simulation starts, the wave kinematics are calculated using stretched Airy theory. Kinematics are calculated up to the instantaneous sea surface. For simulations of irregular sea in the time domain where linear theory does not apply, the user may calculate wave kinematics externally, and give as input for USFOS using the Grid wave option.

The linear/Airy theory applied is described in detail in Usfos theory manual: *USFOS – Hydrodynamics* [3], and in chapter 2.

The wave loads from the simulated sea are calculated using Morison's equation with a nonlinear drag-term. At each time instant, loads are applied up to the instantaneous water surface generated by superposition of the regular wave components. On the basis of the kinematics of each wave component the hydrodynamic loads are calculated as a time series with a given time increment and for a given time interval [3]. When doing dynamic analyses the wave forces are introduced gradually, and the waves are ramped up. That means that in the initiation of the analysis, the first waves that hits the structure is scaled down at t=0, and gradually reach true scale as time increases. The ramp distance is defined by user input in the control file, in the command for *WaveData*.

The formulation of the Morison equation is given below:

$$dF = \rho \frac{\pi D^2}{4} C_M a_n dz + \frac{1}{2} \rho C_D Du |u| ds \quad (5.1)$$

dF = Wave force pr length

ρ = seawater density

D = Cylinder diameter

C_M = mass coefficient

C_D = drag coefficient

u = water particle velocity

a_n = water particle acceleration

ds = unit length

The mass and drag coefficients C_M and C_D , are set to be 1.4 and 2.0 respectively in the analyses done in this report.

When doing dynamic analysis in the time domain for floating structures subject large displacements, the response of the structure will produce waves. Regarding wave kinematics in this situation, the USFOS software can account for this motion by involving the structures relative velocity. This is done by adding the command *rel_velo* in the control file. The velocity terms are then transformed to local element axis system for both structural and wave velocities/accelerations, and the relative values for velocities are calculated and used for calculating actual hydrodynamic loading.

The buoyancy force may be calculated either by determination of the displaced volume (“Archimedes” force) or by direct integration of the hydrostatic - and hydrodynamic pressure over the wetted surface. The latter is used in this work, by the use of command *BUOYFORM PANEL*. Integration of the hydrodynamic pressure gives a reduced buoyancy effect during a wave crest and an increase of the buoyancy during a wave trough compared to the “Archimedes” (static force) force [3]. *BUOYHIST* command defines which elements to be included in the integration of hydrostatic and dynamic pressure. Submerged elements that does not contribute to buoyancy, can be specified with the command *flooded*.

Hydrodynamic mass is accounted for in USFOS, and the mass matrix is constantly updated as the structures moves in the fluid, as only submerged elements contribute to the added mass term.

5.1.2 USFOS other modelling parameters

For post analysis treatment of results, the software package for USFOS called Dynmax is used. The control-file for performing the analysis is coded with specifications for which results one wants to collect. This is done using the *Dynres* commands. Refer USFOS user manual [15] for more details about commands used in the control files. The control file is given in the appendix.

To get response output from usfos that reflects the true dynamic response, one must filter out the transient response observed in the initial phase of the simulation. This is done with the command *ini_time*. With this command one can specify a time for when the software starts recording the output to the result files. This initiation time is set to 500 seconds for all of the simulations done in this work.

5.1.3 Scripting of USFOS

Due to the large amount of simulations done in this work, scripts are created to run consecutive USFOS simulations. The scripts are based on bash scripting technique and developed to be run in a UNIX environment. The scripts can be run on LINUX operating systems standard terminals, or by using the Cygwin terminal in a Windows operating system. The Cygwin terminal is free software available online, and is used simulate a UNIX environment in operating systems other than for example Linux.

The scripts are constructed to make use of specific input regarding parameters for each simulation. This input is then used to substitute a set of parameters inside the control file for the USFOS analysis. The same input is also used for creating folders and storing results in an orderly fashion for easier access when post processing the results. Similar scripts are created for running the post processing modules *dynres* and *dynmax*. Separate scripts are created for each method investigated, and thus one can run them separately.

5.2 MATLAB

MATLAB is used for running statistical analyses of the results, and for writing data to spreadsheets for presentation purposes. It is also used to plot obtained data from the simulations on Gumbel probability paper.

A script *readdynres.m* is created to read all .plo-files obtained from running the *dynres* module. It then proceeds to calculate statistical data for all samples and each method. The calculated data is then written to excel spreadsheets for later evaluation and presentation. Commands for calculating the statistical data are built in functions in MATLAB.

An appendage to the MATLAB software called WAFO is installed. The WAFO appendage is a free MATLAB tool created for statistical calculation of wavedata, and I have made use of the plotting applications available in this tool. Several scripts for plotting Gumbel probability plots are created. They are similar in the way that they read data from the excel sheets created in the *readdynres.m*-script. And differ as they target data from different results in the spreadsheets. The *ygumb.m* and *ygumb2.m* scripts are plotting routines, and scripts *plots.m*, *multiplot.m*, *multi2.m* and *multi3.m* are reading specific data in excel sheets.

MATLAB scripts are also created for generating wave components for input in USFOS. *Randfreq.m* calculates wave components based on FFT-method with random frequency selected within the frequency interval. Calculations are based on JONSWAP spectrum. More details regarding the method are described in chapter 2.5.1. Wave component data are written to 20 sample files for each amount of wave components in use. *rand_freq_amp.m* does a similar routine, but components are calculated according to the method described in chapter 2.5.2, with random Rayleigh distributed wave amplitudes.

Another script and subscript, *gridwave.m* and *gridwrite.m*, creates input files for the grid wave simulations. This script is an elaborate one in terms of calculations. It calculates surface elevation and wave kinematics in time and space for a specified irregular wave field, and writes the data to files for input in USFOS.

All MATLAB scripts include description of variables in use within each script.

6 Case Study – Dynamic response analysis in the time-domain of SWAY tower

This chapter describes the dynamic time-domain simulations performed in this thesis work.

The main objective of the analysis is to investigate the adequacy of different methods to realize the wave spectrum; using the methods FFT, EAP, and FFT with increased randomization of wave frequency and wave component amplitude. In addition to using USFOS for direct calculation of wave kinematics for each load step, pre-calculated wave kinematics tabulated in a grid in time and space are given as input. The amount of necessary wave components for each method is also addressed for each method. All analyses are post processed with statistical evaluation of the wave kinematics and responses found from each simulation.

The structure investigated is the SWAY tower, without a rotating turbine. In place of the turbine are a fixed nodal mass and a fixed node force that represent the loads an, idle turbine would result in.

All simulations with standard FFT and EAP method are carried out in USFOS, with the use of built in JONSWAP wave spectrum as basis for calculating wave components. Spectrum parameters for all analyses are given in chapter 2.4.

Variations of the FFT method, using random frequency (FFT_{rf}) and both random frequency and amplitude (FFT_{rf}_a) when calculating wave components, are also investigated. When giving pre-calculated wave components as input, the components are calculated using MATLAB scripts. The procedure for calculating these wave components are described in detail in chapters 2.5 and 2.6.

A MATLAB script is made for pre-calculation of wave kinematics and generation of grid wave files. The calculations are based on use of linear wave and potential flow theory for establishing wave data. Wheeler stretching is used to establish better estimates of wave kinematics at the sea surface. The wave kinematics and surface elevation is calculated by using the FFT method with random amplitude and wave frequency, as described in chapter 2.5.2. 200 wave components have been used to realize the spectrum.

Altogether, four different methods of realizing the wave spectrum is investigated, and also a fifth method regarding pre-calculation of wave kinematics. The amount of wave components used for each method is varied, and listed in Table 1 on the next page. 20 time series are simulated for each amount of wave components in use. A total of 300 time simulations have been conducted.

Method short name	Simulation length (recorded)	Wave components
FFT	1000	500
		1000
EAP	1000	75
		100
		200
FFTrf	1000	75
		100
		200
		1000
FFTrfa	1000	75
		100
		200
		1000
Grid200 Grid200_1	1000	200
		200

Table 1 – List of methods and variations in wave components

All simulations are carried out for 1500 seconds, and results are recorded for the last 1000 seconds, eliminating any transient response behavior from the result files. The grid wave pre-calculations are based on linear wave theory, and the FFTrfa method with 200 components for realization of the spectrum.

For each time series, the time histories for 6 different parameters are collected and stored:

- Displacement of top of tower(Top disp)
- Acceleration of top of the tower(Top acc)
- Cardan Force
- Moment at middle of tower(Mid moment)
- Surface Elevation
- Total wave load

6.1 Dynamic equation of motion

The general dynamic equation of motion is given as:

$$(A + M)\ddot{\mathbf{u}} + C\dot{\mathbf{u}} + K\mathbf{u} = Q(t) \quad (6.1)$$

Where:

M = mass matrix

A = hydrodynamic added mass, relevant when structure is moving in fluids

C = damping matrix

K = stiffness matrix

Q(t) = deterministic or stochastic load

u = deterministic or stochastic response, and its time-derivatives

In our case we are dealing with a stochastic load, where the wave loads are modelled as a linear combination of several stochastic variables $Q_1(t)$, $Q_2(t)$... and so on.

The dynamic equation of motion is solved to find the structures response to a subjected load. The left hand side of the equation describes the structures/systems mechanical properties, while the right hand side describes the load the system is subjected to. Stiffness and damping properties for a structure is in most cases of nonlinear nature. But this nonlinear behavior will only be of significance when the structure is loaded close to its utilization limit.

The mass and stiffness matrix, **M** and **K**, can be found through interpolation functions. In USFOS, the mass matrix can be formulated either as lumped or consistent. The lumped mass matrix is often used in static analyses, and concentrates mass in specific nodes. This limits the system to only finding nodal displacements in nodes where masses are allocated. The consistent mass matrix includes more node-masses than the lumped mass formulation, and thus it produces more accurate results of the structural response [10]. The consistent mass matrix is often necessary when performing dynamic analysis. The USFOS theory manual describes the process for how this is done using USFOS software [14].

6.2 Damping

The damping coefficient/matrix, \mathbf{C} , in the equation of motion is of high importance. Damping is a structures ability to dissipate kinetic energy into other energy forms[10]. Damping terms are often modelled as linear terms, but when the structure is subjected to loads of extreme magnitude, the response and damping will not behave linearly [2]. It is hard to model damping effects precisely. Simplified estimates of these non-linear damping effects have proven to be satisfactory in many applications [10]. Examples of such estimated damping models are:

- Linear and non-linear viscous damping
- Structural damping (dependent on displacement)
- Coulomb damping (constant damping)
- Rayleigh damping

The Rayleigh model is used in these analyses, and is a built in function in USFOS. The Rayleigh damping is assuming that the damping coefficient is proportional to the mass and stiffness matrix:

$$\mathbf{C} = \alpha_1 \mathbf{M} + \alpha_2 \mathbf{K} \quad (6.2)$$

If the damping ratio is known for two individual structural frequencies, the damping parameters may be chosen as in equations (4.3) and (4.4)[, and the relationship between damping and excitation frequency is given in figure 5:

$$\alpha_1 = \frac{2\omega_1\omega_2}{\omega_1^2 - \omega_2^2} (\lambda_1\omega_2 - \lambda_2\omega_1) \quad (6.3)$$

$$\alpha_2 = \frac{2(\lambda_2\omega_2 - \lambda_1\omega_1)}{\omega_2^2 - \omega_1^2} \quad (6.4)$$

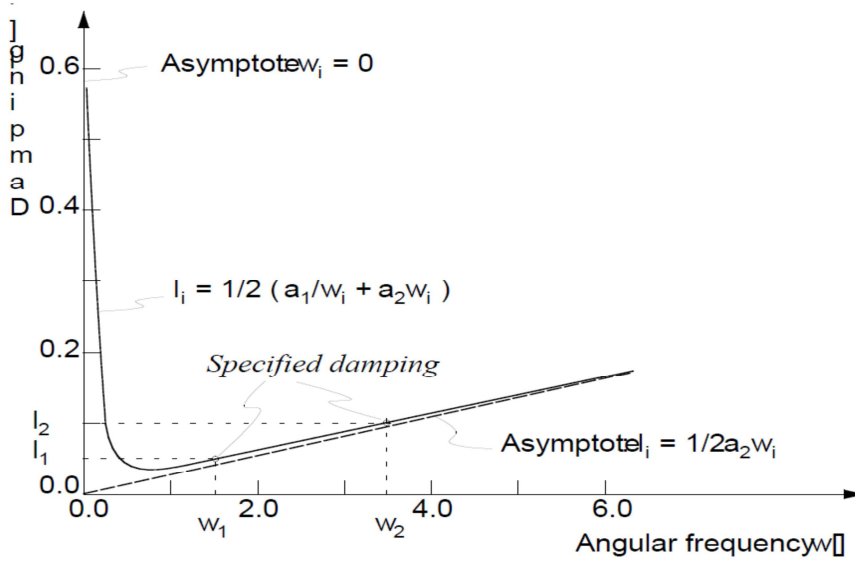


Figure 6 - Damping ratio as function of angular frequency

6.3 Numerical solution of the equation of motion

The USFOS software solves the equation of motion numerically. The method used is one proposed by Hilber, Hughes and Taylor, and is called the HHT- α -method. *The method employs some sort of time averaging of the damping, stiffness and load term expressed by the α -parameter. A beneficial feature of the method is that it introduces artificial damping of higher order frequency modes without degrading the accuracy [14].* The following are excerpts from the USFOS theory manual [14].

The governing equilibrium equation for HHT- α method:

$$M\ddot{r}_{n+1} + (1 + \alpha)C\dot{r}_{n+1} - \alpha C\dot{r}_n + (1 + \alpha)Kr_{n+1} - \alpha Kr_n = (1 + \alpha)R_{n+1} - \alpha R_n \quad (6.5)$$

$$\dot{r}_{n+1} = \dot{r}_n + \Delta t(\gamma)\ddot{r}_n + \Delta t\gamma\ddot{r}_{n+1} \quad (6.6)$$

$$r_{n+1} = r_n + \Delta t\dot{r}_n + \frac{\gamma t^2}{2}(1 - 2\beta)\ddot{r}_n + \Delta t^2\beta\ddot{r}_{n+1} \quad (6.7)$$

The factors, β and γ , are the free parameters in the Newmark- β method which, along with α , determine the stability and accuracy of the quadrature formula.

For the numerical integration to be unconditionally stable, the following conditions must be satisfied:

$$\frac{1}{3} < \alpha < 0 \quad (6.8)$$

$$\gamma = \frac{1}{2}(1 - 2\alpha) \quad (6.9)$$

$$\beta = \frac{1}{4}(1 - \alpha)^2 \quad (6.10)$$

Incremental equations develop as follows:

$$\mathbf{M}(\ddot{\mathbf{r}}_{n+1} - \ddot{\mathbf{r}}_n) + (\mathbf{1} + \alpha)\mathbf{C}(\dot{\mathbf{r}}_{n+1} - \dot{\mathbf{r}}_n) + (\mathbf{1} + \alpha)\mathbf{K}(\mathbf{r}_{n+1} - \mathbf{r}_n) = (\mathbf{1} + \alpha)(\mathbf{R}_{n+1} - \mathbf{R}_n) + \mathbf{R}_n - \mathbf{M}\ddot{\mathbf{r}}_n - \mathbf{C}\dot{\mathbf{r}}_n - \mathbf{K}\mathbf{r}_n \quad (6.11)$$

$$\Delta\ddot{\mathbf{r}}_{n+1} = \ddot{\mathbf{r}}_{n+1} - \ddot{\mathbf{r}}_n = \frac{1}{\Delta t^2\beta}\Delta\mathbf{r}_{n+1} - \frac{1}{\Delta t\beta}\dot{\mathbf{r}}_n - \frac{1}{2\beta}\ddot{\mathbf{r}}_n \quad (6.12)$$

$$\Delta\dot{\mathbf{r}}_{n+1} = \dot{\mathbf{r}}_{n+1} - \dot{\mathbf{r}}_n = \frac{\gamma}{\Delta t\beta}\Delta\mathbf{r}_{n+1} - \frac{\gamma}{\beta}\dot{\mathbf{r}}_n - \Delta t\left(\frac{\gamma}{2\beta} - \mathbf{1}\right)\ddot{\mathbf{r}}_n \quad (6.13)$$

Combining eqs. 6.11 to 6.13 yields only $\Delta\mathbf{r}_{n+1}$ as unknown. When ordered with unknown at left hand side, the resulting equation becomes:

$$\left[(\mathbf{1} + \alpha)\mathbf{K} + (\mathbf{1} + \alpha)\frac{\gamma}{\Delta t\beta}\mathbf{C} + \frac{1}{\Delta t^2\beta}\mathbf{M} \right] \Delta\mathbf{r}_{n+1} = (\mathbf{1} + \alpha)(\mathbf{R}_{n+1} - \mathbf{R}_n) + \mathbf{R}_n - \mathbf{M}\ddot{\mathbf{r}}_n - \mathbf{C}\dot{\mathbf{r}}_n - \mathbf{K}\mathbf{r}_n + \left[\frac{1}{\Delta t\beta}\dot{\mathbf{r}}_n + \frac{1}{2\beta}\ddot{\mathbf{r}}_n \right] \mathbf{M} + \left[(\mathbf{1} + \alpha)\left(\frac{\gamma}{\beta}\dot{\mathbf{r}}_n + \Delta t\left(\frac{\gamma}{2\beta} - \mathbf{1} \right) \right) \ddot{\mathbf{r}}_n \right] \mathbf{C} \quad (6.14)$$

When $\Delta\mathbf{r}_{n+1}$ is known, the displacement, velocity and acceleration can be found:

$$\mathbf{r}_{n+1} = \mathbf{r}_n + \Delta\mathbf{r}_{n+1} \quad (6.15)$$

$$\dot{\mathbf{r}}_{n+1} = \frac{\gamma}{2\beta}\Delta\mathbf{r}_{n+1} + \left(\mathbf{1} - \frac{\gamma}{\beta} \right) \dot{\mathbf{r}}_n - \Delta t\left(\frac{\gamma}{2\beta} - \mathbf{1} \right) \ddot{\mathbf{r}}_n \quad (6.16)$$

$$\Delta\ddot{\mathbf{r}}_{n+1} = \frac{1}{\Delta t^2\beta}\Delta\mathbf{r}_{n+1} - \frac{\gamma}{\Delta t\beta}\dot{\mathbf{r}}_n + \left(\mathbf{1} - \frac{1}{2\beta} \right) \ddot{\mathbf{r}}_n \quad (6.17)$$

6.4 Dynamic analysis of SWAY tower

The model and control file

The model and control file used throughout this thesis work, is given as a digital attachment to the report. Key information about the model and analysis control commands is described in this chapter:

The sway tower main body is 194 meters tall, with the lowermost part being submerged 100 meters below the stillwater surface. A mooring line, 50 meters long, is modelled as a flexible pipe is connecting the anchor swivel to seabed. The water depth for the analyses is thus 150 meters. The tower diameter is varying along the height of the tower. For the submerged part, the minimum diameter is 7.3 meters, and maximum diameter 9.3 meters. From the surface and up, the tower diameter is 4.5m. The diameter at the sea surface is around 5 meters, and wave loads are thus mass dominated.

The model is exposed to fixed nodal loads, resembling the wind forces that would act on an otherwise installed wind turbine. In this model, this turbine is removed, and a vertical nodal mass load has replaced it.

NOTE: The model remains unchanged for all dynamic analyses, except for the analyses based on the use a grid wave. When the grid wave is used as wave data, the buoyancy forces lose its effect, and a fixed node load of 50 MN is replacing the buoyancy force. This simplification does mean that the response of the tower, when exposed to the grid wave, will be of a different nature than for the other methods.

JONSWAP spectrum is used for all wave component and kinematics calculations, with spectrum parameters $H_s=16.4$ m, $T_p=17$ s, and $\gamma=3.3$.

The grid wave method is investigated with to different resolutions of the wave kinematic data file. Grid200 has between 50-70 nodes in vertical direction, and 28 nodes in horizontal x-direction. The spacing between nodes in the vertical direction is 0.2 m in close to surface and around wave crest and wave trough, but of much lower resolution closer to the seabed. The vertical resolution is unchanged for grid200_1 input, but the horizontal resolution is halved.

7 Results and Discussion

To find the accuracy of the methods used to simulate irregular sea, a statistical evaluation of the time histories must be done. The surface elevation process is of high interest to study closely, and results from the structural response are also investigated for each method. The extreme values of these different time histories are of greatest interest to examine, as these values often are the magnitude for which a response analysis is concluded on. Results from each method is presented, and discussed in separate subchapters.

7.1 Verification of results

The most thorough analysis done is this work, which by previous studies resembles the truest irregular sea, is the FFT method with 1000 components. The results from this analysis will serve as the correct results, and the other methods are compared upon.

Sample statistics in this report is based on available data for 20 time histories for each method. This is regarded as a sufficient amount of samples necessary to conduct conclusive statistical review of each method. Gumbel plots are created for further evaluation of extreme values for both surface elevation process, and structural responses. Short term variability in the results will be present in the results, and deviations are expected.

The statistical evaluation of the surface elevation process for each method, will be compared against the statistical properties for a true Gaussian distributed variable. A Gaussian distributed variable will have expected mean value $E[X]=0$, skewness=0 and kurtosis=3. The wave peaks for a stationary Gaussian distributed wave profile is Rayleigh distributed [5]. Then the relationship between significant wave height H_s , and the standard deviation σ is given as:

$$H_s = H_{1/3} = 4\sqrt{m_0} = 4\sigma \rightarrow \sigma = \frac{H_s}{4} \quad (7.1)$$

The formulas for calculating mean, variance, skewness and kurtosis for a sample are given in chapter 3.

Data for the complete time series have been stored in result files created by usfos. *Dynres* module has been used to export the data to text files, which is later imported and analyzed in MATLAB. The calculations of statistical parameters in MATLAB makes use of built in functions for calculating maximums, mean, variance, skewness, kurtosis and standard deviation. Gumbel plots are created for extreme value samples for wave height, waveload, cardan force, midmoment, and horizontal displacement and acceleration at the top of the tower.

Simulations are carried out with several different methods. In the presentation of the results, the methods are identified by short names:

FFT1000 – spectrum realization using the constant $d\omega$ method, with 1000 components

FFT500 – constant $d\omega$, 500 components

EAP75 – equal area principle, varying $d\omega$, 75 components

EAP100 – varying $d\omega$, 100 components

EAP200 – varying $d\omega$, 200 components

FFTrf75 – constant $d\omega$, random frequency within $d\omega$ interval, 75 components

FFTrf100 – constant $d\omega$, random frequency within $d\omega$ interval, 100 components

FFTrf200 – constant $d\omega$, random frequency within $d\omega$ interval, 200 components

FFTrf1000 – constant $d\omega$, random frequency within $d\omega$ interval, 1000 components

FFTrfa75 – constant $d\omega$, random frequency and amplitude, 75 components

FFTrfa100 – constant $d\omega$, random frequency and amplitude, 100 components

FFTrfa200 – constant $d\omega$, random frequency and amplitude, 200 components

FFTrfa1000 – constant $d\omega$, random frequency and amplitude, 1000 components

grid200 – Gridwave, pre-calculated kinematics as input, linear theory, resolution $dx=5$ m

grid200_1 – Gridwave, pre-calculated kinematics as input, linear theory, resolution $dx=10$ m

7.2 Results of surface elevation process

7.2.1 Surface elevation process, numerical results

Collected stats surface profile						mean	max	std
method	mean value	variance	skewness	kurtosis	Std dev	maximum	maximum	maximums
FFT1000	-0,006	17,31	-0,006	2,95	4,15	13,10	17,08	1,81
FFT500	-0,008	16,35	0,012	2,97	4,04	13,09	15,96	1,83
EAP75	0,001	16,52	-0,008	3,03	4,06	12,57	16,70	1,74
EAP100	0,000	16,72	-0,038	2,94	4,08	12,35	15,71	1,67
EAP200	-0,004	16,10	-0,010	2,94	4,00	11,86	16,96	1,76
FFTrf75	-0,004	16,29	-0,020	2,76	4,03	11,80	15,16	1,36
FFTrf100	0,004	16,87	-0,023	2,83	4,10	12,44	15,47	1,32
FFTrf200	0,002	16,68	-0,014	3,04	4,08	12,82	14,94	1,15
FFTrf1000	-0,006	17,55	-0,002	2,91	4,18	12,51	15,22	1,15
FFTrfa75	0,002	16,08	-0,008	2,72	3,96	11,48	13,82	1,75
FFTrfa100	0,000	15,54	-0,016	2,82	3,91	11,79	17,53	1,98
FFTrfa200	0,003	17,76	-0,007	2,95	4,18	12,65	18,22	2,13
FFTrfa1000	-0,001	16,43	0,008	2,89	4,05	12,12	14,68	1,35
grid200	-0,001	15,71	0,046	2,78	3,94	12,04	15,16	1,84
grid200_1	-0,003	16,96	-0,023	2,91	4,09	12,33	15,75	1,78

Table 2 - Collected statistics of elevation process, all methods

Table 2 presents averages calculated for the surface elevation process from all samples, for each method. Two separate columns at the far right show the highest maximum recorded for the method, and the standard deviation for the maximums sample from each method. Full results from surface elevation process are given for each method in appendix.

7.2.2 Gumbel plots of extreme value distribution of wave heights.

Gumbel plots are created for extreme value distributions of the wave height. Figures 8 to 21 shows the fitted Gumbel probability papers for the maximum distributions of surface elevation for all methods.

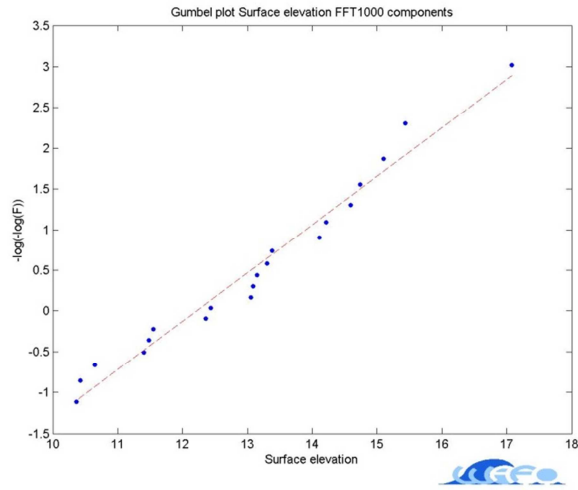


Figure 7 - Gumbel plot FFT1000 - maximum distribution of surface elevation

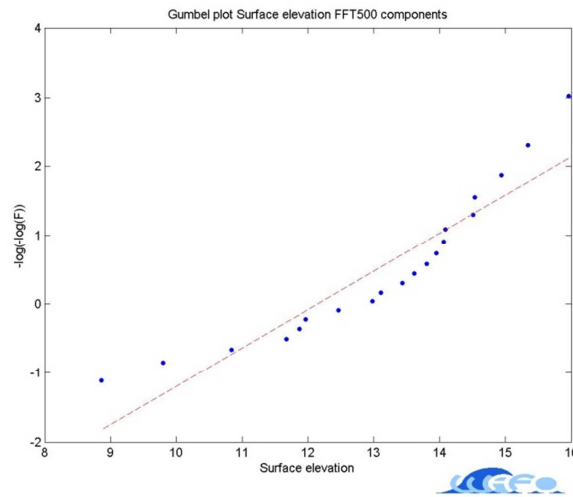


Figure 8 - Gumbel plot FFT500 - maximum distribution of surface elevation

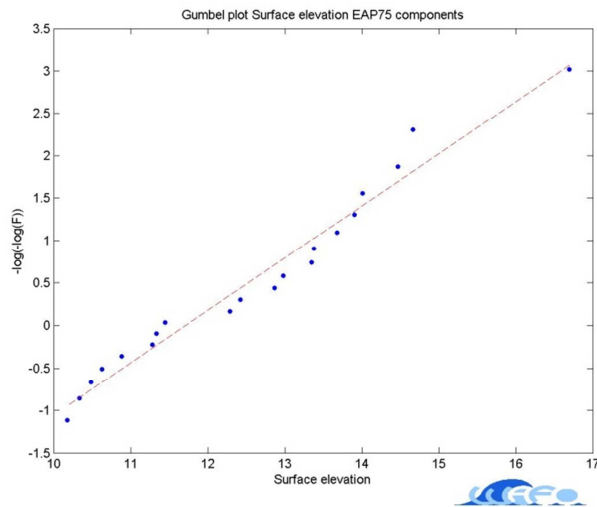


Figure 9 - Gumbel plot EAP75 - maximum distribution of surface elevation

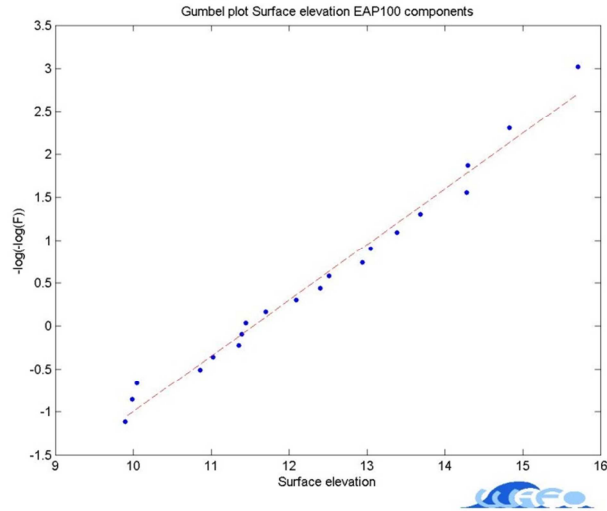


Figure 10 - Gumbel plot EAP100 - maximum distribution of surface elevation

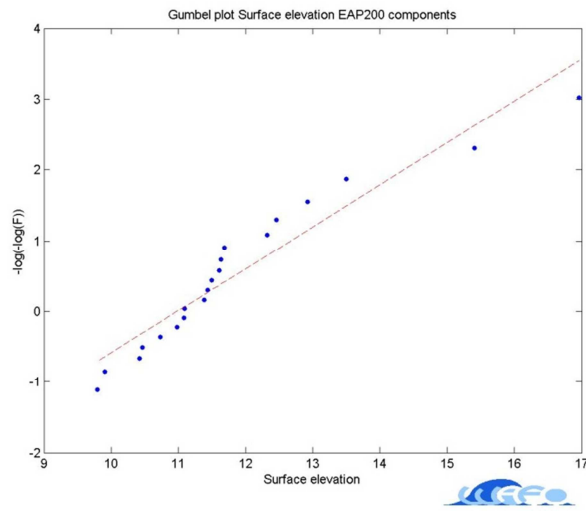


Figure 11 - Gumbel plot EAP200 - maximum distribution of surface elevation

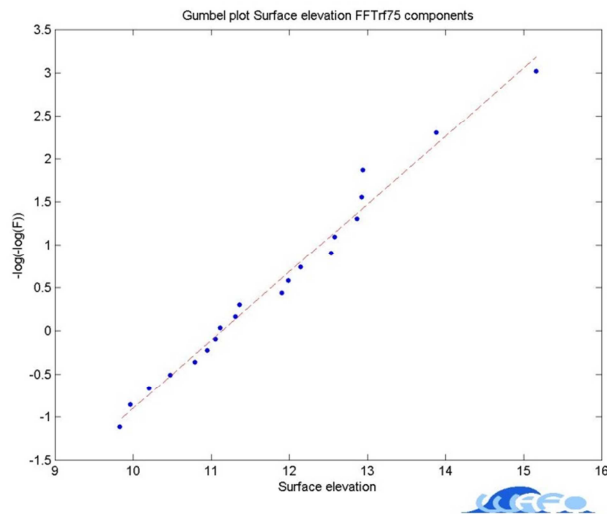


Figure 12 - Gumbel plot FFTrf75 - maximum distribution of surface elevation

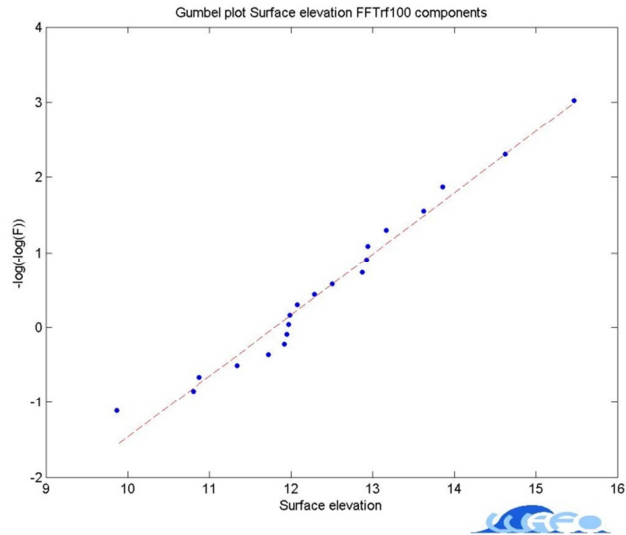


Figure 13 - Gumbel plot FFTrf100 - maximum distribution of surface elevation

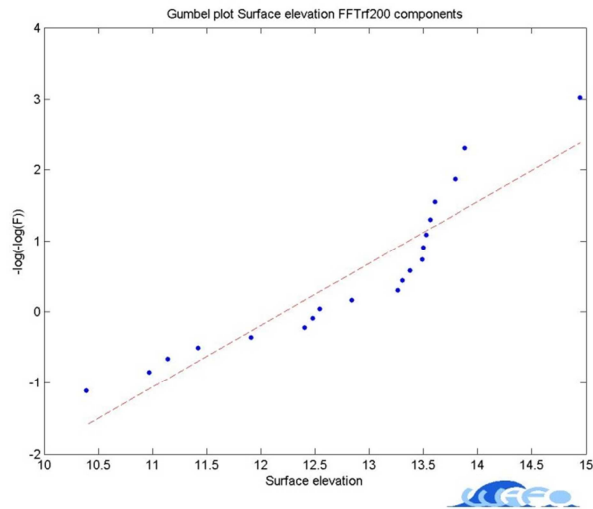


Figure 14 - Gumbel plot FFTrf200 - maximum distribution of surface elevation

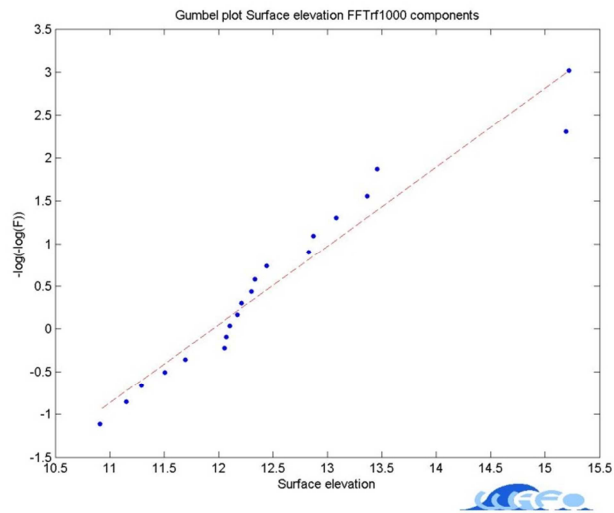


Figure 15 - Gumbel plot FFTrf1000 - maximum distribution of surface elevation

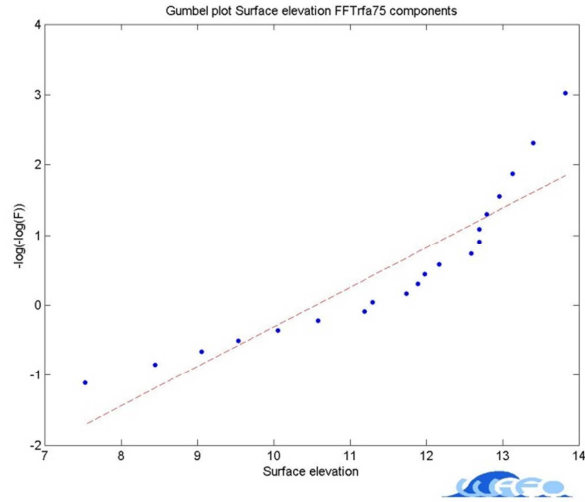


Figure 16 - Gumbel plot FFTrfa75 - maximum distribution of surface elevation

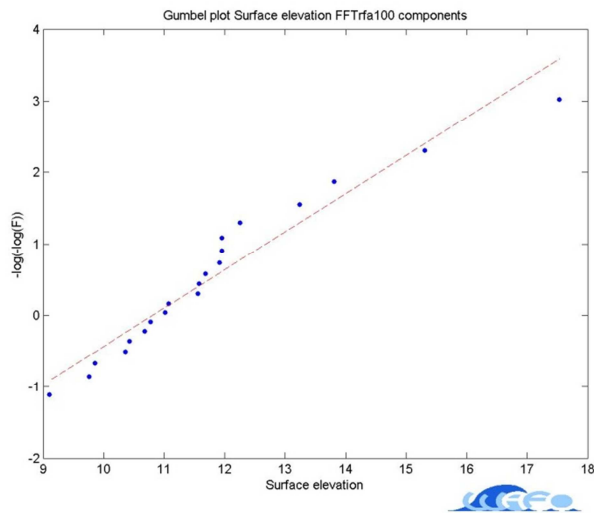


Figure 17 - Gumbel plot FFTrfa100 - maximum distribution of surface elevation

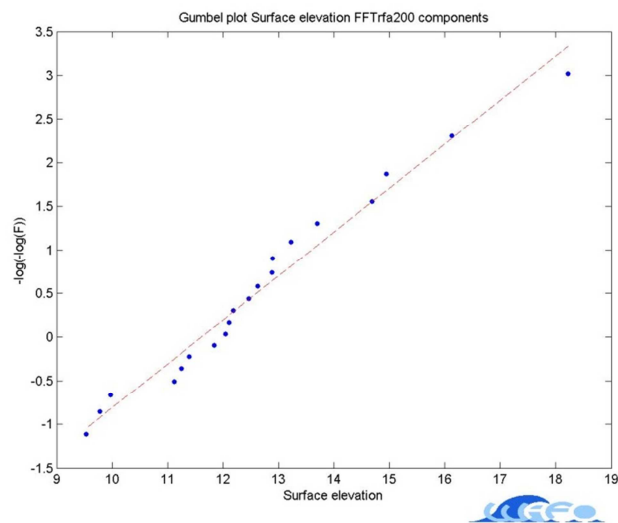


Figure 18 - Gumbel plot FFTrfa200 - maximum distribution of surface elevation

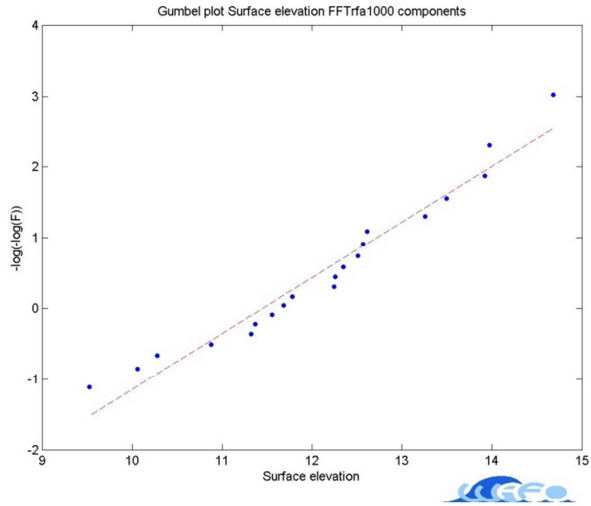


Figure 19 - Gumbel plot FFTrfa1000 - maximum distribution of surface elevation

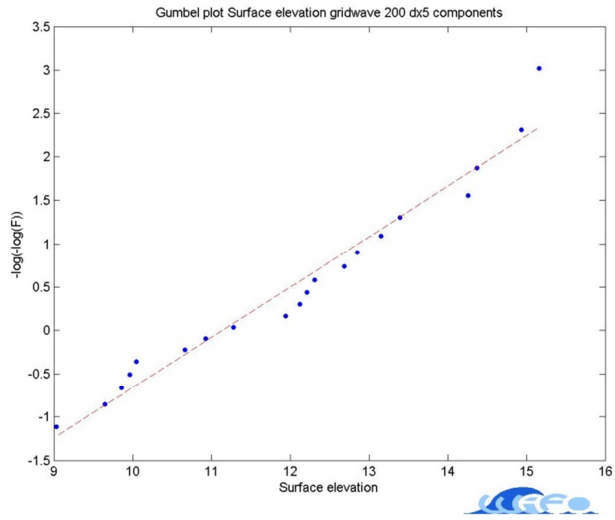


Figure 20 - Gumbel plot grid200 - maximum distribution of surface elevation

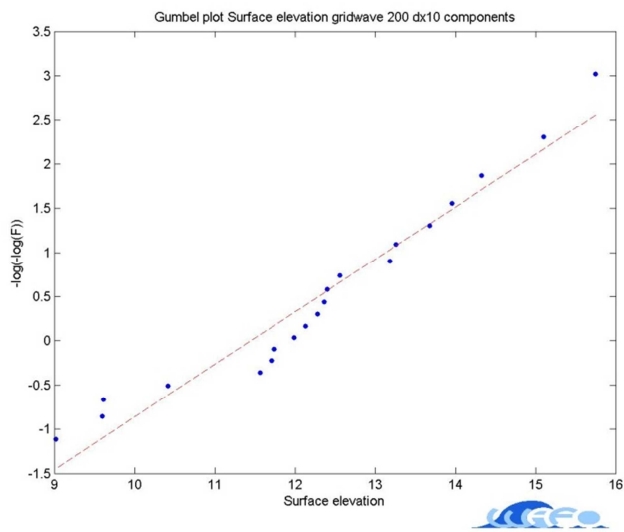


Figure 21 - Gumbel plot grid200_1 - maximum distribution of surface elevation

7.3 Discussion of surface elevation process results

The simulated elevation processes should, if modelled correctly, approach the Gaussian distribution. For the Gaussian distribution the theoretic statistical parameters are given in Table 3. The Variance and standard deviation are calculated using the relationship between H_s and standard deviation as given in equation (7.1) The statistical parameters of the elevation process are discussed in this chapter.

Theoretical values Gaussian distribution $H_s=16.4$				
mean	variance	skewness	kurtosis	Std dev
0	16,81	0	3	4,1

Table 3 - Theoretical values of statistical parameters, Gaussian sea with $H_s=16.4$ m

7.3.1 Mean value of surface profile

The expected mean for a Gaussian distributed variable should be zero. The average mean value for all samples are given in Table 2. The calculated mean values for each method is satisfactory for all the methods investigated. The standard deviation of the mean for each method is found to be in the range 0.011 to 0.016. This also suggests that the mean value is stable close to zero for all simulation methods.

7.3.2 Standard deviation/Variance

The significant wave height H_s is set to 16.4 meters for all simulations. The theoretic standard deviation for a Gaussian distributed elevation is thus 4.1m as given in table 3, calculated from eq (7.1). The average standard deviation for each method is listed in Table 2, and is satisfactory for all methods, as the highest deviation from the theoretical value is no more than 4.2%

The method which depicts a standard deviation furthest from the theoretical value is the FFT methods based on both random frequency and amplitude for 75 components. The grid wave input is based on the same calculation method for establishing wave components, and this simulation also depicts a standard deviation lower than the true Gaussian. The reason for this deviation is most likely the increased randomization of parameters used for calculating the wave component amplitudes. The deviation is shown to be larger the fewer components that is used. Very accurate results for the FFTrf and FFTrfa are obtained for simulations done with 200 components.

7.3.3 Kurtosis / flatness parameter

For a true Gaussian distribution of the surface elevation, the kurtosis should be equal to 3.

The average kurtosis value found from each method is shown in table 2. It is observed that most of the methods show good resemblance to the theoretic value of the kurtosis parameter. Though for the FFTrf and FFTrfa methods with 75 components, the kurtosis value is deviating with almost 10%. The kurtosis parameter has increased accuracy when wave components are increased for both methods.

When comparing the standard deviations of the kurtosis parameter for each individual time history for each method, the parameters are varying with a range 0.2-0.29 for all methods. This is due to making use only 20 samples for each method.

7.3.4 Skewness parameter

The skewness parameter for the Gaussian distribution is equal to zero. The average skewness parameter for each method is given in table 2, and shows satisfactory values very close to the theoretic value.

7.3.5 Extreme value statistics of surface elevation

The distribution of maxima is assumed to be a narrow-banded process. The adequacy of this assumption is supported [6] [7]. Assuming all wave peaks are identically distributed, and statistically independent of each other, then the distribution of individual maxima follows the Rayleigh distribution

The Rayleigh distribution for wave peaks ξ , with standard deviation σ :

$$f_{\xi}(\xi) = \frac{\xi}{\sigma^2} \exp\left\{-\frac{1}{2}\left(\frac{\xi}{\sigma}\right)^2\right\} \quad (7.2)$$

The theoretical extreme value for the wave peak generated from a JONSWAP spectrum with $H_s=16.4m$, is calculated using the level crossing period and the duration of the simulation. If the above assumptions hold, the formula for calculating the maximum wave peak for a process with zero level crossing period T_0 and a given duration T is given in eq (7.3)

$$\xi_{1/3} = \sigma \left(\left(\sqrt{2 \ln\left(\frac{T}{T_0}\right)} \right) + \frac{0.5772}{\sqrt{2 \ln\left(\frac{T}{T_0}\right)}} \right) = 12.85m \quad (7.3)$$

The average values of the observed maximum surface elevation for each method are listed in Table 2, along with the highest observed maximum elevation in a single time series for each method. The standard FFT method slightly over predicts the maximum wave elevation for both 1000 and 500 components, when compared to the theoretical value calculated in eq (7.3), while most of the other methods slightly under predicts the maximums. There is statistical uncertainties linked to the calculated theoretic maximum in (7.3), as it rests on the assumption that the peak distribution being narrow-banded.

It is also observed that the FFTrf75 and FFTrfa75 simulations under predicts the maximum wave elevation by over 10%. For these methods of simulation, the kurtosis value was 2.76 and 2.72 respectively. The kurtosis value describes the shape of the probability density distribution, and a kurtosis value less than three will give a distribution that is more flat at the peak. This low kurtosis value for the sample tells us that the peak values are under estimated when comparing against the theoretic Gaussian distribution with kurtosis value 3. The results from FFTrf- and FFTrfa-methods improve when more components are used, and for components 200 or more, the observed maximums are the closest to the theoretic values.

Figures 8 to 21 shows the extreme value distribution for all methods. A trend observed is that the more components used for the simulations, a better fit for the gumbel plot is seen. Most plots show good results regarding the distribution of maxima, as the highest concentration of observations lie around the theoretic extreme value from eq (7.3).

When comparing each method and the amount of components used, it is observed that EAP method produce decent results for all variations. FFTrf and FFTrfa methods show consistently good results for 200 components or more. Using less components than 100 for the latter two methods is not advised, as this produces large under estimations of the surface elevation.

7.4 Results wave loads from dynamic analysis of SWAY tower

Averages of total wave load from each method are produced in table 4, as well as average of maximums, and average standard deviation. 20 samples for each method form the basis of the produced results. Ratios when compared to FFT1000 are given in table 5.

Collected stats waveloads				mean
method	mean value	variance	Stnd dev	maximum
FFT1000	2,96E+04	2,42E+13	4,91E+06	1,60E+07
FFT500	2,10E+04	2,29E+13	4,78E+06	1,63E+07
EAP75	2,07E+04	2,29E+13	4,78E+06	1,60E+07
EAP100	2,94E+04	2,33E+13	4,82E+06	1,60E+07
EAP200	2,08E+04	2,25E+13	4,72E+06	1,50E+07
FFTrf75	1,76E+04	2,28E+13	4,77E+06	1,49E+07
FFTrf100	3,49E+04	2,36E+13	4,86E+06	1,53E+07
FFTrf200	2,60E+04	2,33E+13	4,82E+06	1,63E+07
FFTrf1000	2,58E+04	2,46E+13	4,95E+06	1,63E+07
FFTrfa75	2,07E+04	2,26E+13	4,70E+06	1,43E+07
FFTrfa100	1,44E+04	2,19E+13	4,65E+06	1,47E+07
FFTrfa200	2,82E+04	2,49E+13	4,95E+06	1,64E+07
FFTrfa1000	2,53E+04	2,31E+13	4,80E+06	1,59E+07
grid200	5,19E+03	9,94E+12	3,13E+06	9,71E+06
grid200_1	1,40E+04	1,07E+13	3,26E+06	9,77E+06

Table 4- Results from dynamic analysis - Total Wave Load

Ratio of FFT1000, waveloads			Mean
method	mean value	Stnd dev	maximum
FFT1000	1,00	1,00	1,00
FFT500	0,71	0,97	1,02
EAP75	0,70	0,97	1,00
EAP100	0,99	0,98	1,00
EAP200	0,71	0,96	0,94
FFTrf75	0,59	0,97	0,93
FFTrf100	1,18	0,99	0,96
FFTrf200	0,88	0,98	1,02
FFTrf1000	0,87	1,01	1,02
FFTrfa75	0,70	0,96	0,90
FFTrfa100	0,49	0,95	0,92
FFTrfa200	0,95	1,01	1,02
FFTrfa1000	0,85	0,98	1,00
grid200	0,18	0,64	0,61
grid200_1	0,47	0,66	0,61

Table 5 - Wave load ratio, compared against results from FFT1000 method

Gumbel plots for the extreme value distribution of total wave load for each method are created, collecting all variations regarding amount of components for each method inside the same plot. The plots are shown in figure 22 to 26.

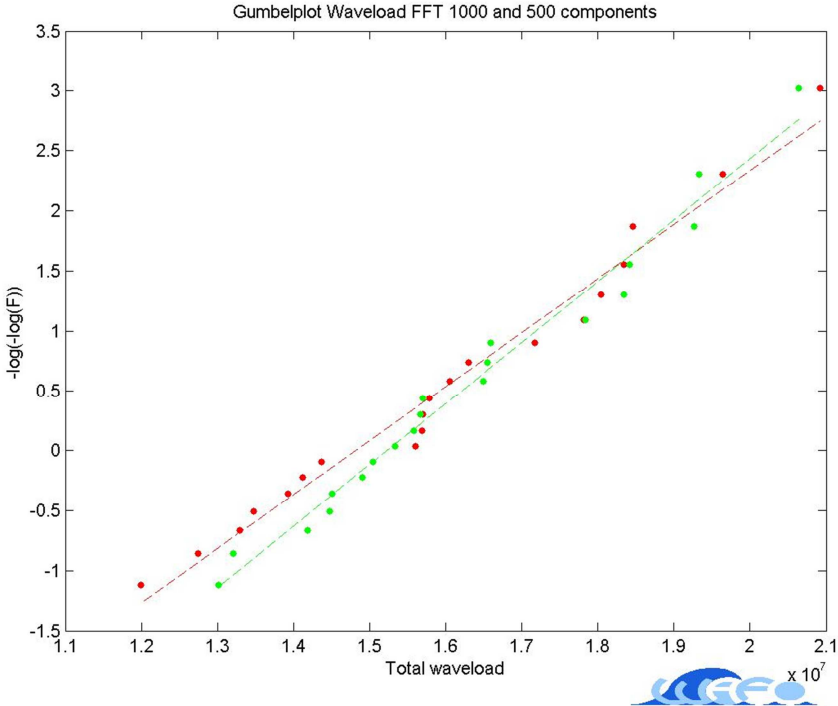


Figure 22 - Gumbel plot FFT 1000 and 500, Total waveload

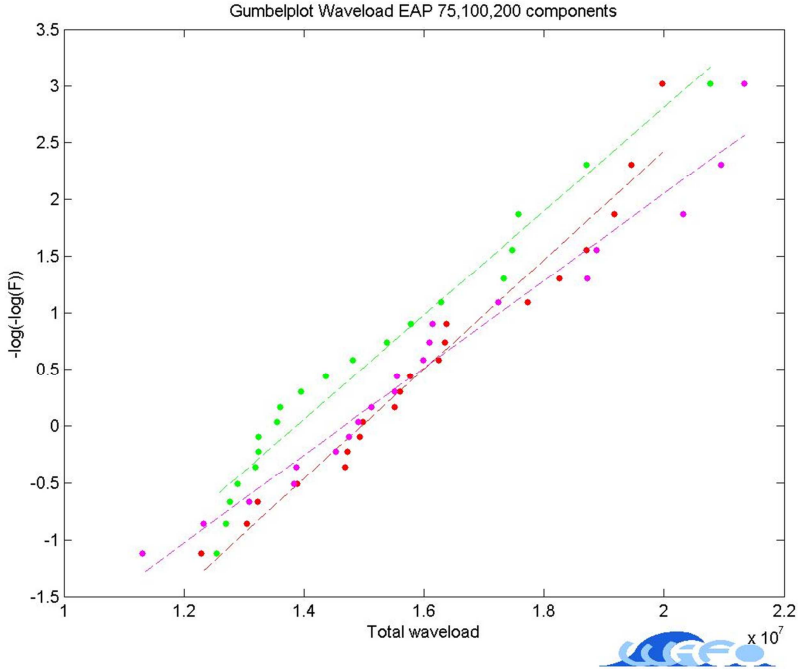


Figure 23 - Gumbel plot EAP method - Total wave load

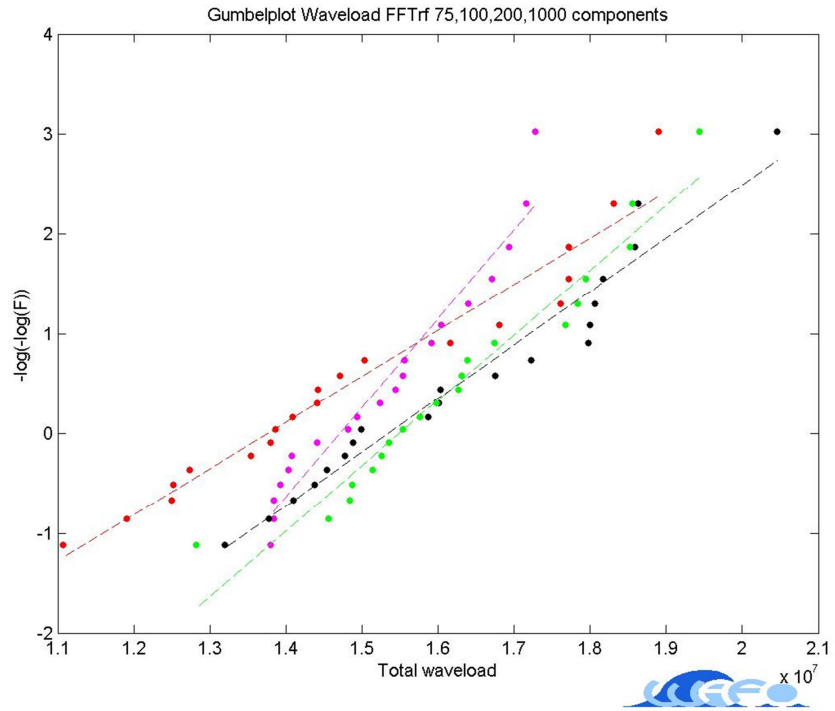


Figure 24- Total wave load FFTrf method

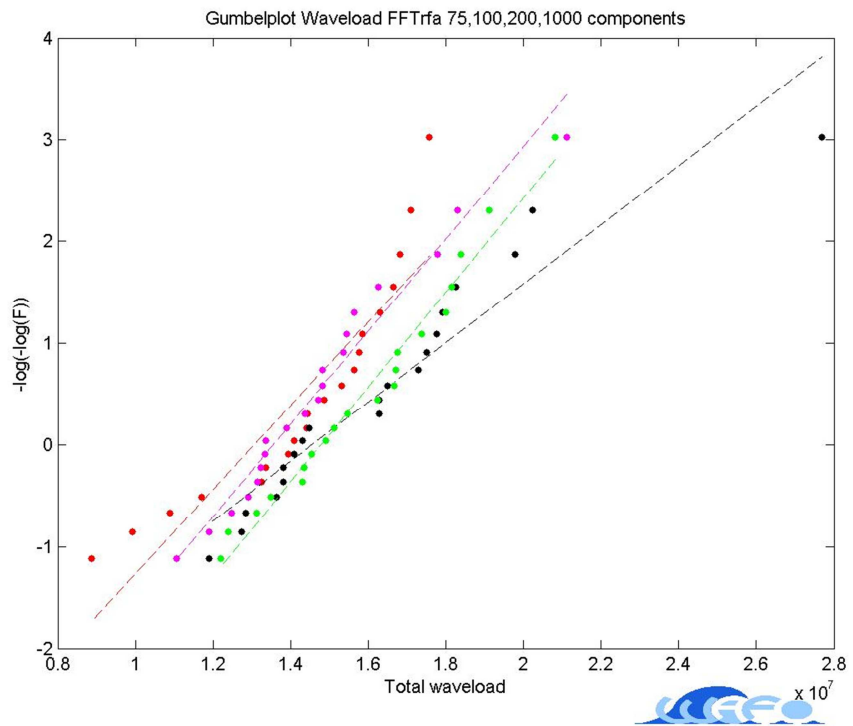


Figure 25- Total wave load FFTrfa method

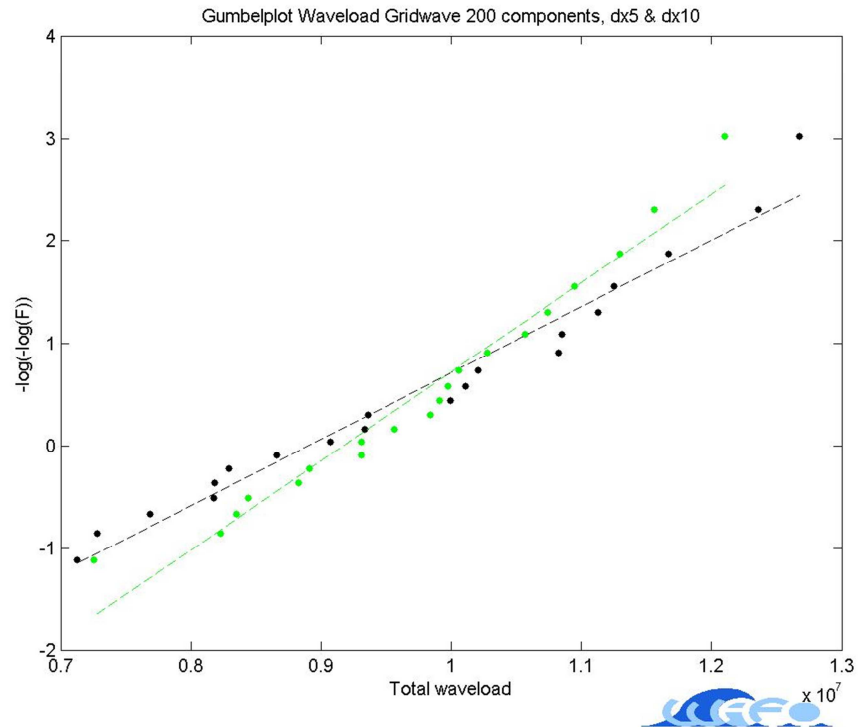


Figure 26 - Total wave load Grid wave method 200 components

7.5 Discussion results total wave load

The average maximum total wave load obtained from each method is listed in table 4. When comparing to the FFT method (Table 5), few ratios stand out. The EAP method produces almost identical results to the FFT method when using 100 components. The FFTrf and FFTrfa methods also produce good results when compared, and the best outcome when looking at the wave components used for the two methods, are simulations using 200 components or more

As expected, the grid wave method is producing a not so similar load history, as for the other methods. This is due to complications during analyses. The grid wave method did not support how the buoyancy was modelled for the tower. And the buoyancy was replaced with a static load. This has produced a whole different load history for the dynamic analysis, and results cannot be compared against the FFT 1000 method. When comparing the grid wave methods up against each other, the difference in resolution of wave kinematic calculations shows negligible effect. It is necessary to research this matter further.

7.6 Results dynamic analysis of SWAY tower - response

7.6.1 Numeric results from dynamic analysis of SWAY tower - response

Table 6 shows collected averages of results obtained from the dynamic response analysis of the sway tower, and standard deviation for the observed magnitudes. Table 7 shows ratios of obtained results when compared against the FFT 1000 results.

Method	Cardan Force [N]		Midmoment [Nm]		acc. Top tower[m/s ²]		displ top tower [m]	
	Stnd dev	maximum	Stnd dev	maximum	Stnd dev	maximum	Stnd dev	maximum
FFT1000	7,39E+05	4,23E+06	7,67E+07	2,04E+08	1,62	5,15	10,92	37,37
FFT500	7,27E+05	4,23E+06	7,54E+07	2,08E+08	1,59	5,30	10,66	38,99
EAP75	7,22E+05	4,24E+06	7,45E+07	2,12E+08	1,58	5,28	10,40	39,42
EAP100	7,28E+05	4,30E+06	7,53E+07	1,99E+08	1,59	5,20	10,56	31,92
EAP200	7,15E+05	4,25E+06	7,40E+07	1,95E+08	1,57	4,95	10,37	32,36
FFTrf75	7,22E+05	4,22E+06	7,47E+07	1,92E+08	1,58	4,95	10,50	36,24
FFTrf100	7,35E+05	4,26E+06	7,63E+07	1,96E+08	1,61	5,03	10,83	39,56
FFTrf200	7,29E+05	4,21E+06	7,60E+07	2,12E+08	1,60	5,33	10,92	41,84
FFTrf1000	7,46E+05	4,26E+06	7,73E+07	2,09E+08	1,64	5,30	10,95	39,48
FFTrfa75	7,15E+05	4,22E+06	7,39E+07	1,91E+08	1,57	4,88	10,34	36,39
FFTrfa100	7,10E+05	4,22E+06	7,33E+07	1,92E+08	1,56	4,94	10,19	31,71
FFTrfa200	7,48E+05	4,28E+06	7,77E+07	2,07E+08	1,64	5,30	11,06	43,67
FFTrfa1000	7,29E+05	4,17E+06	7,54E+07	2,05E+08	1,59	5,16	10,61	37,09
grid200	4,16E+05	5,84E+06	7,88E+07	1,97E+08	1,56	4,27	9,15	20,57
grid200_1	4,59E+05	6,02E+06	8,27E+07	2,07E+08	1,63	4,45	9,63	21,93

Table 6 - Averages of response from dynamic analysis of sway tower

Method	Cardan Force [N]		Midmoment [Nm]		acc. Top tower[m/s ²]		displ top tower [m]	
	Std dev	maximum	Std dev	maximum	Std dev	maximum	Std dev	maximum
FFT1000	1,00	1,00	1,00	1,00	1,00	1,00	1,00	1,00
FFT500	0,98	1,00	0,98	1,02	0,98	1,03	0,98	1,04
EAP75	0,98	1,00	0,97	1,04	0,98	1,03	0,95	1,06
EAP100	0,98	1,02	0,98	0,98	0,98	1,01	0,97	0,85
EAP200	0,97	1,00	0,97	0,96	0,97	0,96	0,95	0,87
FFTrf75	0,98	1,00	0,97	0,94	0,98	0,96	0,96	0,97
FFTrf100	0,99	1,01	1,00	0,96	0,99	0,98	0,99	1,06
FFTrf200	0,99	0,99	0,99	1,04	0,99	1,03	1,00	1,12
FFTrf1000	1,01	1,01	1,01	1,02	1,01	1,03	1,00	1,06
FFTrfa75	0,97	1,00	0,96	0,94	0,97	0,95	0,95	0,97
FFTrfa100	0,96	1,00	0,96	0,94	0,96	0,96	0,93	0,85
FFTrfa200	1,01	1,01	1,01	1,01	1,01	1,03	1,01	1,17
FFTrfa1000	0,99	0,99	0,98	1,01	0,98	1,00	0,97	0,99
grid200	0,56	1,38	1,03	0,96	0,96	0,83	0,84	0,55
grid200_1	0,62	1,42	1,08	1,01	1,01	0,86	0,88	0,59

Table 7 - Ratios of response results when compared against results from FFT 1000 method

7.6.2 Gumbel plots for extreme value distributions of response

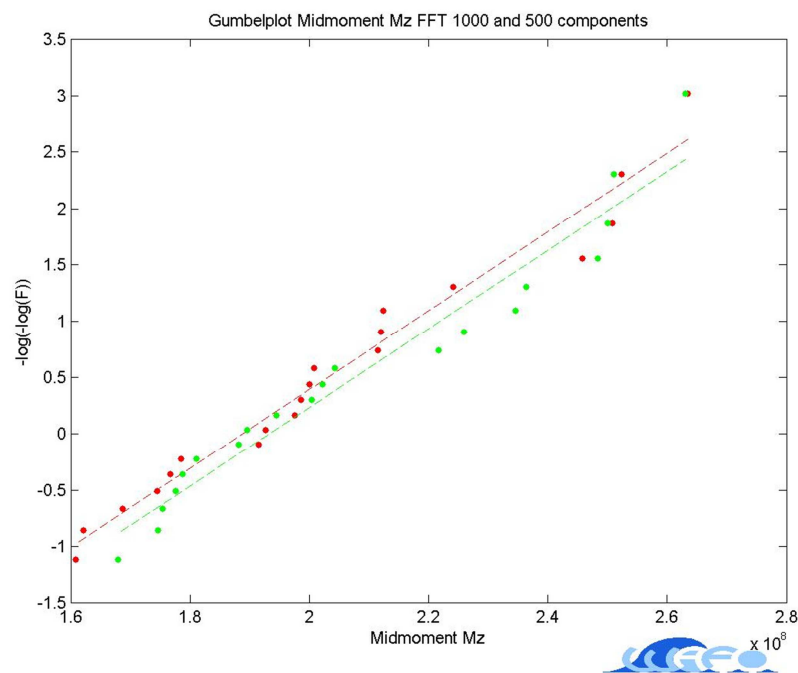


Figure 27 - Gumbel plot Midmoment Mz FFT method

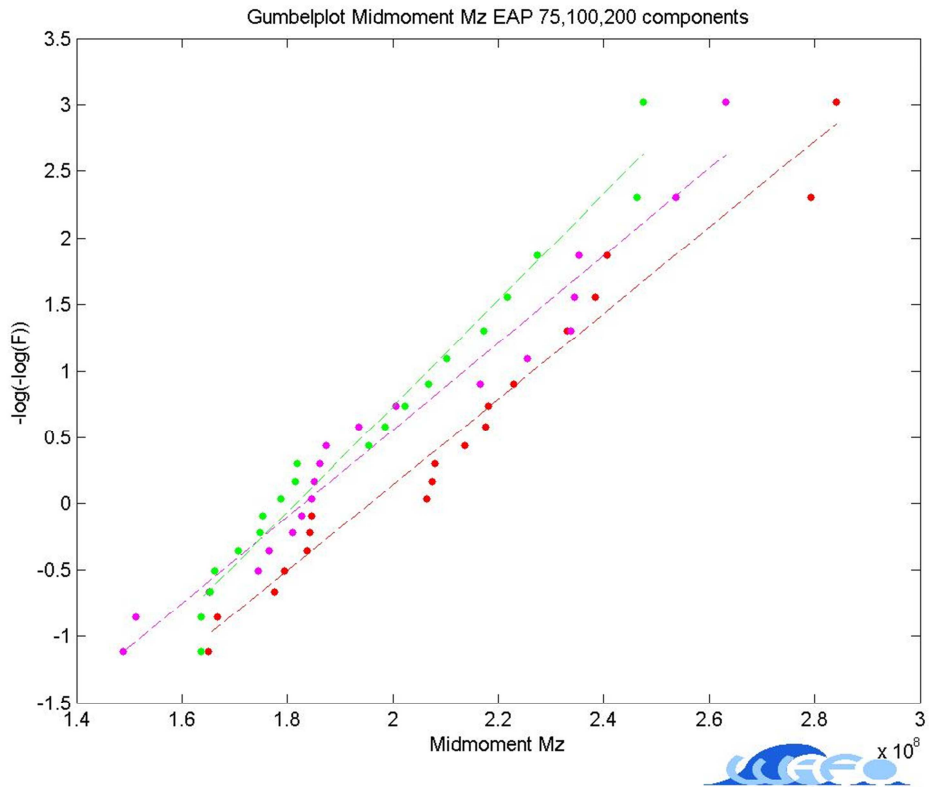


Figure 28 - Gumbel plot - Midmoment Mz EAP method

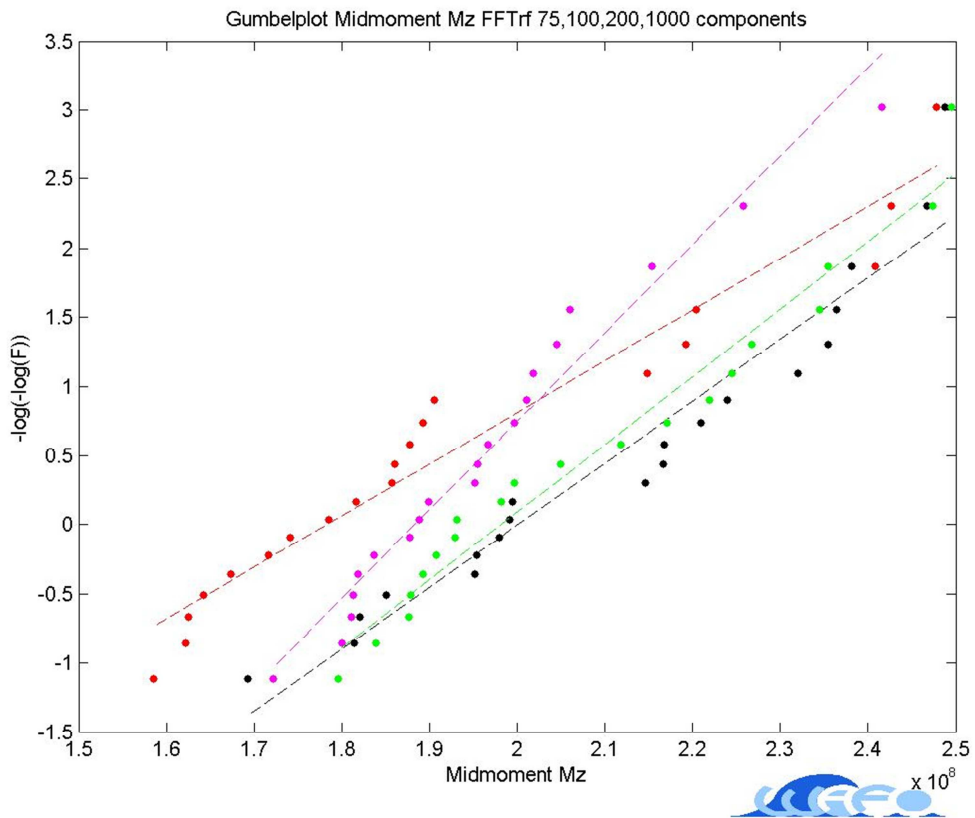


Figure 29 - Gumbel plot - Midmoment Mz FFTrf method

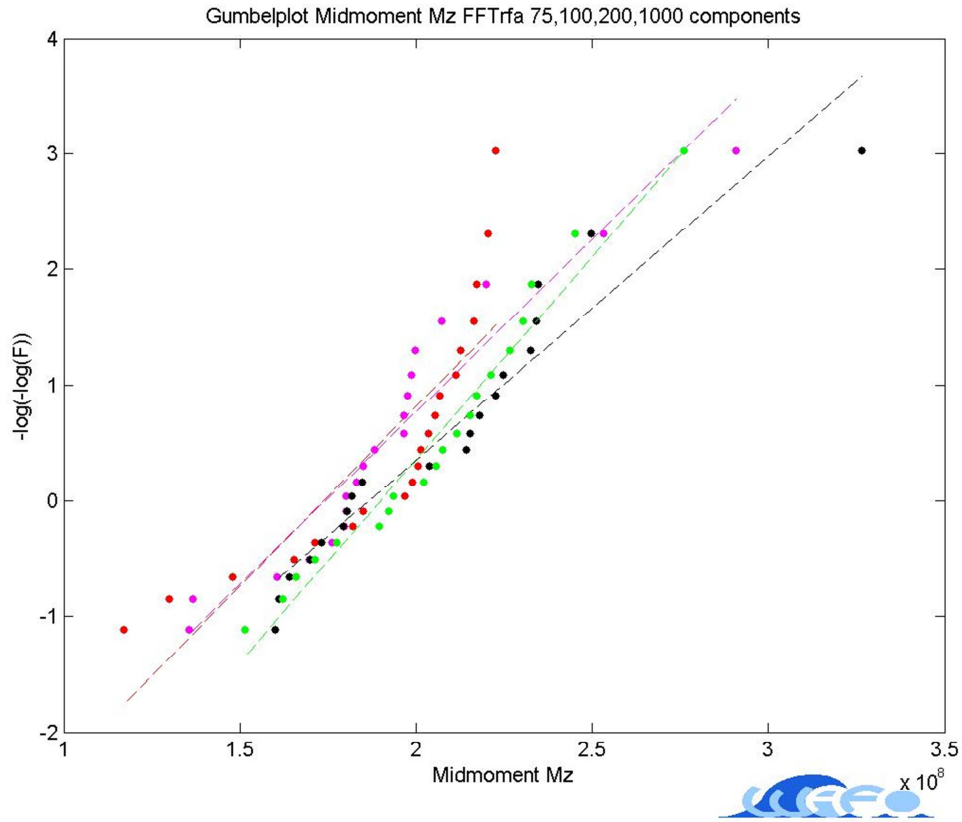


Figure 30 - Gumbel plot - Midmoment Mz FFTrfa method

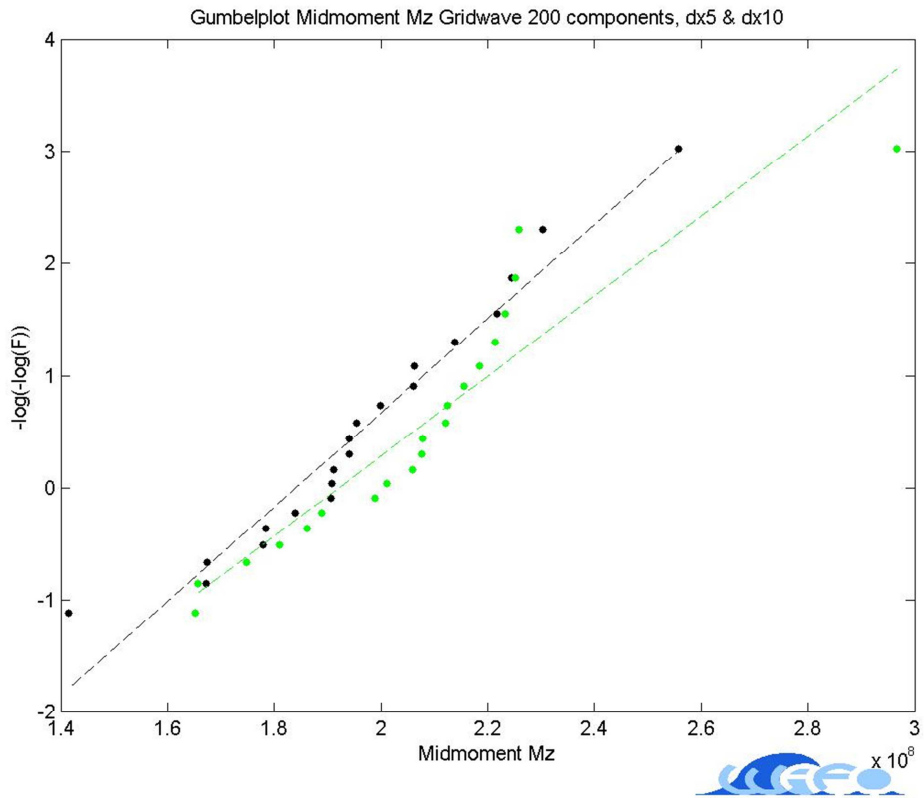


Figure 31 - Gumbel plot - Midmoment Gridwave method

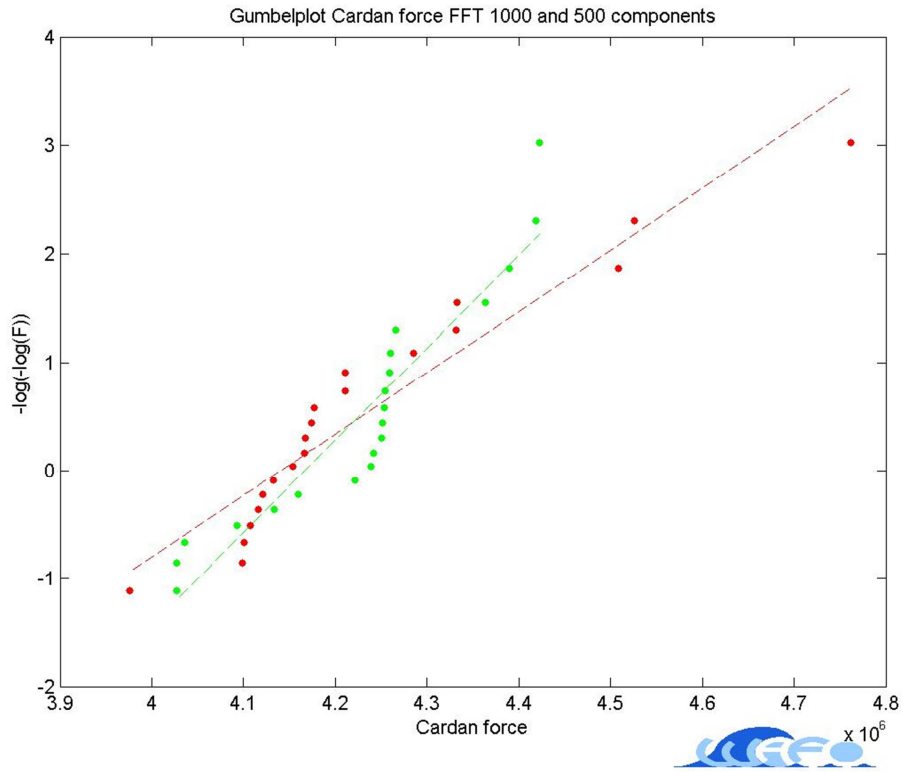


Figure 32 - Gumbel plot - Cardan force FFT method

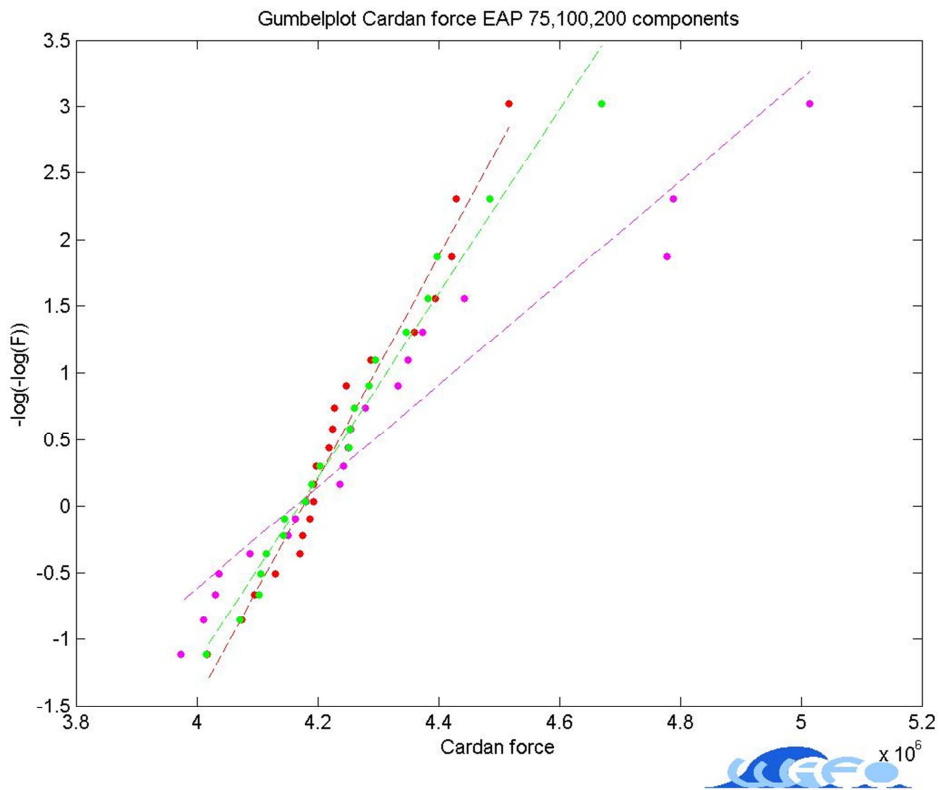


Figure 33 - Gumbel plot Cardan force - EAP method

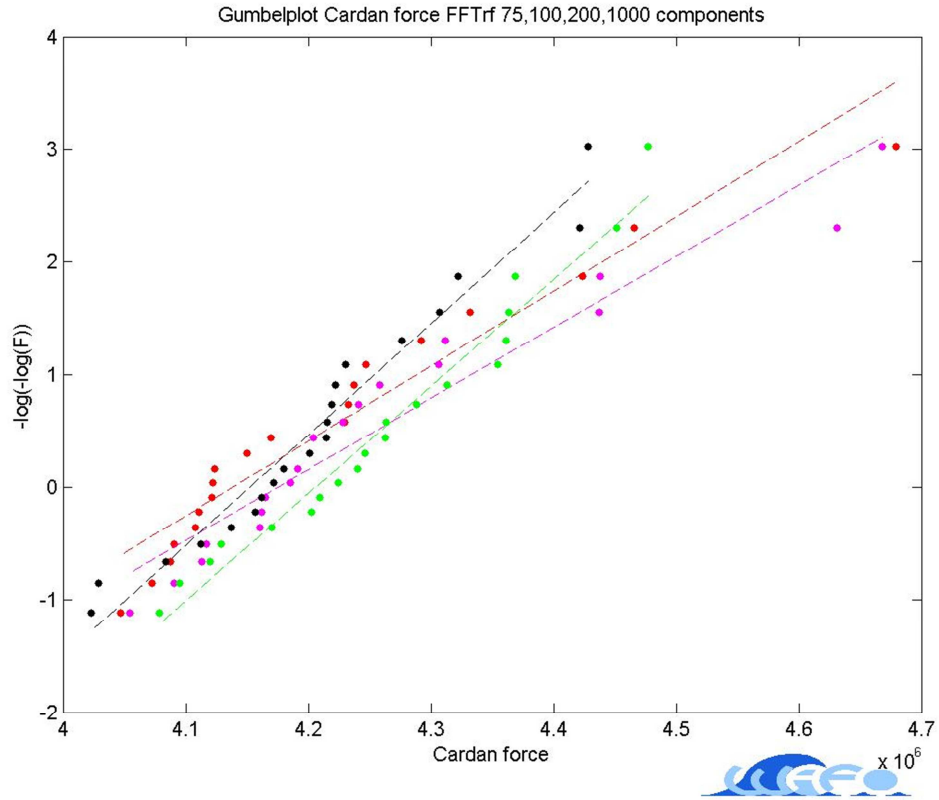


Figure 34 - Gumbel plot - Cardan force FFTrf method

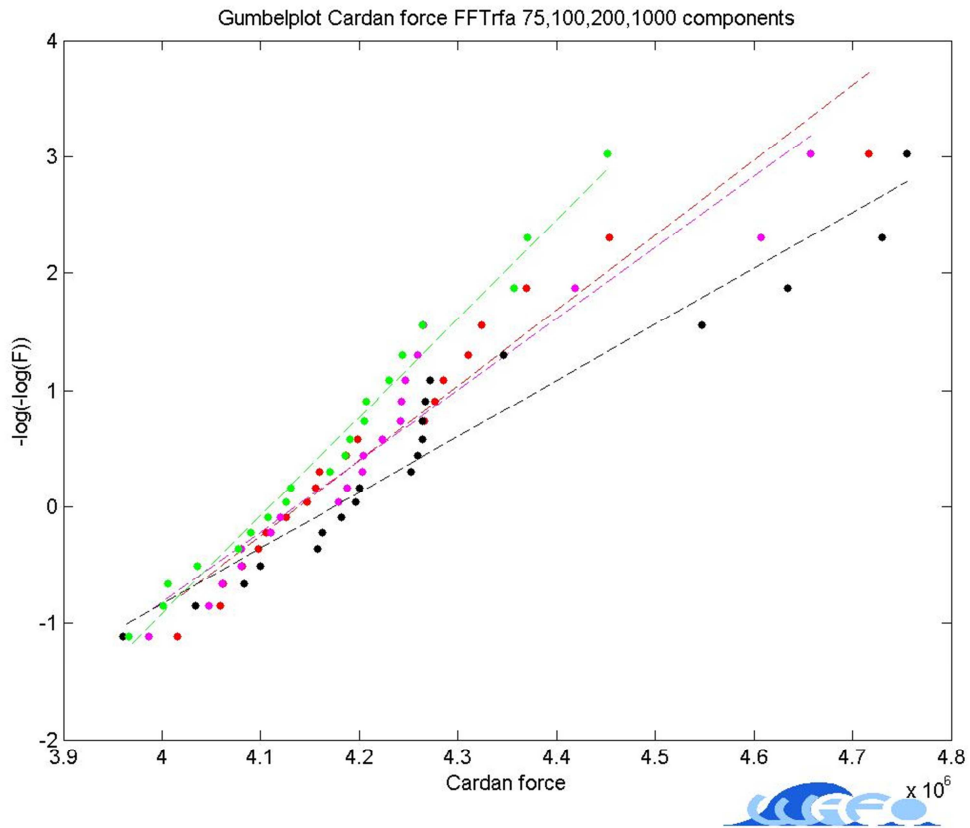


Figure 35 - Gumbel plot - Cardan force FFTrfa method

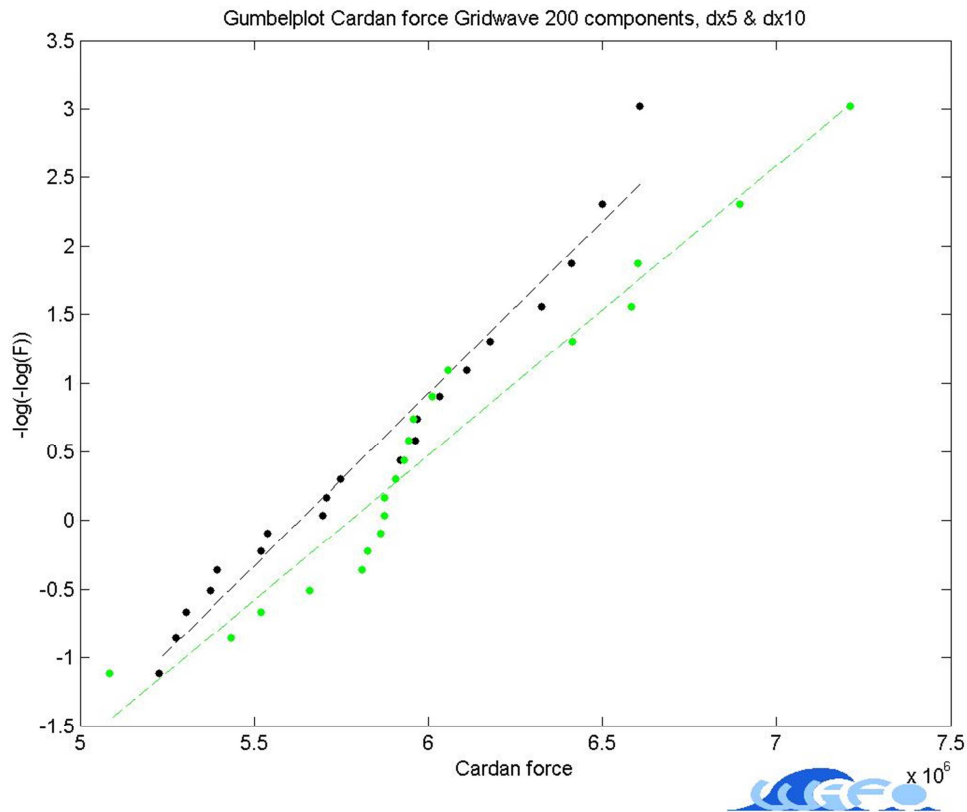


Figure 36 - Gumbel plot - Cardan force - Gridwave method

7.7 Discussion of Response analysis results SWAY tower

It is observed that the EAP methods over predicts the responses when amount of components used is little. For EAP method with 100 and 200 components, the forces and displacements are under predicted. When EAP method is used for few wave components, the surface elevation will have peaks that are over predicted. This will lead to larger wave loads and responses. When several components are used with this method, the lower and higher frequencies of the wave spectrum will not be represented in high resolution. The effects of this might be the reason for the under prediction of the responses for EAP method with 200 components. This is supported by the results from the cardan force as the natural period in heave for the sway tower is around 1 second.

The FFTrf and FFTrfa methods show very good accuracy when the amount of components is 200 or more. For 100 components or less, the response results will be under predicted. The grid wave results are incomparable with rest of the methods due to different loading situation.

7.7.1 Slow-drift motions and sum frequency effects in irregular waves

Slow-drift motions are resonance oscillations excited by nonlinear interaction between the waves and body motion [1][4]. The damping of the sway tower is low, and thus large displacements occur. When the mean wave loads are large, so are the slow-drift excitation loads, and can be of equal importance [4]. Equation (7.4) express the slow-drift effects[1]:

$$F_i^{SV} = \sum_{j=1}^N \sum_{k=1}^N A_j A_k \left[T_{jk}^{ic} \cos \left((\omega_k - \omega_j)t + (\epsilon_k - \epsilon_j) \right) + T_{jk}^{is} \sin \left((\omega_k - \omega_j)t + (\epsilon_k - \epsilon_j) \right) \right] \quad (7.4)$$

A=Wave amplitude

ω = wave frequency

ϵ = phase angle

T= 2nd order transfer function

N= number of wave components

t= time

Due to nonlinear effects, one gets excitation forces with higher frequencies than the dominant frequencies in the wave spectrum. This is because of terms oscillating with frequencies $2\omega_j$, $2\omega_k$ and $(\omega_k + \omega_j)$, where ω is the wave frequency. These effects might be important for exciting the resonance oscillations in heave, pitch and roll of the tower. These loads are however much smaller than the wave frequency loads [4].

8 Conclusion

The EAP method is showing good results for simulation of irregular sea. It resembles a close to true Gaussian sea even with components as low as 75. It is not however, a very good method for dynamic response analysis for the SWAY tower. With 75 components used to simulate the sea, the responses are over predicted compared to that of a standard FFT solution, using 1000 components. When components are increased up to 200, the result is under prediction of responses. The reason for the over prediction of responses when EAP components are few, is that the method produces higher average wave amplitudes. The under prediction of response in the dynamic simulation of the sway tower when wave components increase, might be due to lower representation of the most high and low wave frequencies in the spectrum.

The FFT method using randomly selected frequencies within the ω -interval when calculating wave components show very good surface realization for wave components 200 or more. When fewer wave components than 100 are used, the kurtosis is far too low for resembling a true Gaussian sea. When few components are used with this method, the wave loads and responses are under predicted. When 200 components are used, the method shows close to exact same results as for standard FFT with 1000 components.

The same goes for the FFTrfa method, where wave components are calculated using random frequency selected as with FFTrf method, and Rayleigh distributed wave amplitude. This method also shows large deviations when using few wave components. The FFTrfa with 75 components came out with the poorest results when compared to standard FFT using 1000 components, both for the surface realization and response analysis.

The results obtained using FFTrf and FFTrfa method with 1000 components does also follow the FFT solution. Giving support to the observation that 200 components is satisfactory for obtaining accurate results from time domain response analysis with duration 1000 seconds.

The grid wave method was not a successful investigation in this report. The modelled buoyancy forces did not work properly when using this method, and a simplified replacement of this force was obtained by use of a node load. The load scenario for the model was changed very much with this adjustment, and thus it was rendered incomparable to the other methods. The method was investigated with varying resolution of the wave field containing data for wave kinematics. The resolution was reduced to half of its initial, without experiencing a very large change in results.

9 Recommendation for further work.

The analyses based on use of a grid wave as input for USFOS did not pan out well. Modelling of buoyancy forces that are applicable when using this method for USFOS input must be addressed.

Statistical uncertainties will always be present when performing numerical response analysis in the time domain. Further studies regarding the statistical accuracy for using EAP should be done.

10 References

- [1] O.M. Faltinsen, *Sea Loads on Ships and Offshore Structures*, Cambridge 1990
- [2] Sverre Haver, Prediction of characteristic response, Statoil/Trondheim 2011
- [3] USFOS theory, *hydrodynamics*, www.usfos.no
- [4] Binner, Ine Therese - Master thesis in Marine Tech. 2011, *Time-domain simulations of wind power plants in irregular seas*, NTNU, Trondheim 2011
- [5] Dag Myrhaug, *Kompendium TMR4180 Marin Dynamikk – Uregelmessig sjø*, NTNU, Trondheim 2007
- [6] Bernt Leira, *Probabilistic Modelling and Estimation*, NTNU, Trondheim 2005
- [7] Dag Myrhaug, Kompendium TMR4235 Stochastic theory of sealoading – Statistics of Narrow Band Processes and Equivalent Linearization, NTNU, Trondheim 2005
- [8] R. Zhao, O. M. Faltinsen, *A comparative study of theoretical models for slowdrift motion of a marine structure*, NTNU, Trondheim 1988
- [9] SWAY A/S, *The SWAY concept*, www.sway.no
- [10] Langen/Sigbjørnson, *Dynamisk analyse av konstruksjoner*, SINTEF, Trondheim 1979
- [11] Bjørnar Pettersen, *Marin teknikk 3 – Hydrodynamikk*
- [12] J.D. Wheeler, *Method for calculating forces produced by irregular waves*
- [13] Eivind Bækkedal, *Alternative methods of realizing the sea spectrum for time domain simulation of marine structures in irregular seas*, NTNU 2014
- [14] Tore H. Søreide, Jørgen Amdahl, Ernst Eberg, Tore Holmås, Øyvind Hellan, *USFOS theory manual, USFOS – A computer program for progressive collapse analysis of steel offshore structures*, Rev. 1993 – Trondheim
- [15] USFOS, *USFOS users manual - Input description USFOS control parameters*, www.usfos.no
- [16] USFOS, *USFOS user manual – USFOS wave kinematics file format*
- [17] M.J. Tucker et al. – *Numerical Simulation of random sea ; a common error and its effect upon wave group statistics*, Applied ocean research, vol. 6, no.2, 1984
- [18] USFOS – *Getting Started*, Trondheim 2001
- [19] WAFO group, *Wafo tutorial* - <http://www.maths.lth.se/matstat/wafo/documentation/>, Lund University

[20] DNV-GL, Recommended practice DNV-RP-205

S. Elgar – *Wave group statistics from numerical simulations of a random sea*, Scripps institute of oceanography, University of California, La Jolla, California, 1985

Appendix

A.1 data files/usfos/matlab/bash

Usfos control and model files are attached as digital appendage to the report, together with matlab routines, and bash scripts for running usfos in systematic execution of simulations. Bash scripts are created for each method investigated.

A.2 Complete results

A.2.1 Averages collected from all methods

Collected stats surface profile [m]						mean	max	std
method	mean value	variance	skewness	kurtosis	Std dev	maximum	maximum	maximums
FFT1000	-0,006	17,31	-0,006	2,95	4,15	13,10	17,08	1,81
FFT500	-0,008	16,35	0,012	2,97	4,04	13,09	15,96	1,83
EAP75	0,001	16,52	-0,008	3,03	4,06	12,57	16,70	1,74
EAP100	0,000	16,72	-0,038	2,94	4,08	12,35	15,71	1,67
EAP200	-0,004	16,10	-0,010	2,94	4,00	11,86	16,96	1,76
FFTTrf75	-0,004	16,29	-0,020	2,76	4,03	11,80	15,16	1,36
FFTTrf100	0,004	16,87	-0,023	2,83	4,10	12,44	15,47	1,32
FFTTrf200	0,002	16,68	-0,014	3,04	4,08	12,82	14,94	1,15
FFTTrf1000	-0,006	17,55	-0,002	2,91	4,18	12,51	15,22	1,15
FFTTrfa75	0,002	16,08	-0,008	2,72	3,96	11,48	13,82	1,75
FFTTrfa100	0,000	15,54	-0,016	2,82	3,91	11,79	17,53	1,98
FFTTrfa200	0,003	17,76	-0,007	2,95	4,18	12,65	18,22	2,13
FFTTrfa1000	-0,001	16,43	0,008	2,89	4,05	12,12	14,68	1,35
grid200	-0,001	15,71	0,046	2,78	3,94	12,04	15,16	1,84
grid200_1	-0,003	16,96	-0,023	2,91	4,09	12,33	15,75	1,78

Theoretical values Gaussian distribution Hs=16.4m				
mean	variance	skewness	kurtosis	Std dev
0	16,81	0	3	4,1

Collected stats waveloads [N]				mean
method	mean value	variance	Stnd dev	maximum
FFT1000	2,96E+04	2,42E+13	4,91E+06	1,60E+07
FFT500	2,10E+04	2,29E+13	4,78E+06	1,63E+07
EAP75	2,07E+04	2,29E+13	4,78E+06	1,60E+07
EAP100	2,94E+04	2,33E+13	4,82E+06	1,60E+07
EAP200	2,08E+04	2,25E+13	4,72E+06	1,50E+07
FFTrf75	1,76E+04	2,28E+13	4,77E+06	1,49E+07
FFTrf100	3,49E+04	2,36E+13	4,86E+06	1,53E+07
FFTrf200	2,60E+04	2,33E+13	4,82E+06	1,63E+07
FFTrf1000	2,58E+04	2,46E+13	4,95E+06	1,63E+07
FFTrfa75	2,07E+04	2,26E+13	4,70E+06	1,43E+07
FFTrfa100	1,44E+04	2,19E+13	4,65E+06	1,47E+07
FFTrfa200	2,82E+04	2,49E+13	4,95E+06	1,64E+07
FFTrfa1000	2,53E+04	2,31E+13	4,80E+06	1,59E+07
grid200	5,19E+03	9,94E+12	3,13E+06	9,71E+06
grid200_1	1,40E+04	1,07E+13	3,26E+06	9,77E+06

Collected stats accel top tower [m/s ²]				mean
method	mean value	variance	Stnd dev	maximum
FFT1000	0,000	2,630	1,619	5,150
FFT500	-0,001	2,540	1,592	5,299
EAP75	-0,001	2,503	1,581	5,280
EAP100	0,002	2,542	1,593	5,205
EAP200	-0,001	2,477	1,570	4,953
FFTrf75	-0,002	2,510	1,583	4,954
FFTrf100	0,003	2,596	1,610	5,031
FFTrf200	0,000	2,561	1,600	5,329
FFTrf1000	-0,001	2,683	1,635	5,301
FFTrfa75	-0,001	2,496	1,566	4,883
FFTrfa100	-0,002	2,440	1,556	4,941
FFTrfa200	-0,001	2,716	1,640	5,296
FFTrfa1000	0,000	2,550	1,595	5,159
grid200	-0,001	2,468	1,557	4,272
grid200_1	0,001	2,706	1,633	4,453

Collected stats disp top tower [m]				mean
method	mean value	variance	Stnd dev	maximum
FFT1000	-1,95	119,93	10,92	37,37
FFT500	0,31	114,01	10,66	38,99
EAP75	0,16	108,64	10,40	39,42
EAP100	-6,21	112,11	10,56	31,92
EAP200	-3,79	109,00	10,37	32,36
FFTrf75	-0,14	110,68	10,50	36,24
FFTrf100	1,01	117,68	10,83	39,56
FFTrf200	2,82	119,39	10,92	41,84
FFTrf1000	0,84	120,69	10,95	39,48
FFTrfa75	1,12	110,60	10,34	36,39
FFTrfa100	-2,78	105,76	10,19	31,71
FFTrfa200	4,14	124,86	11,06	43,67
FFTrfa1000	-0,98	113,29	10,61	37,09
grid200	-1,72	85,66	9,15	20,57
grid200_1	-1,38	94,64	9,63	21,93

Collected stats cardan force [N]				mean
method	mean value	variance	Stnd dev	maximum
FFT1000	2,70E+06	5,49E+11	7,39E+05	4,23E+06
FFT500	2,71E+06	5,30E+11	7,27E+05	4,23E+06
EAP75	2,71E+06	5,23E+11	7,22E+05	4,24E+06
EAP100	2,71E+06	5,31E+11	7,28E+05	4,30E+06
EAP200	2,71E+06	5,13E+11	7,15E+05	4,25E+06
FFTrf75	2,71E+06	5,22E+11	7,22E+05	4,22E+06
FFTrf100	2,70E+06	5,42E+11	7,35E+05	4,26E+06
FFTrf200	2,71E+06	5,32E+11	7,29E+05	4,21E+06
FFTrf1000	2,69E+06	5,59E+11	7,46E+05	4,26E+06
FFTrfa75	2,71E+06	5,21E+11	7,15E+05	4,22E+06
FFTrfa100	2,72E+06	5,08E+11	7,10E+05	4,22E+06
FFTrfa200	2,69E+06	5,65E+11	7,48E+05	4,28E+06
FFTrfa1000	2,71E+06	5,33E+11	7,29E+05	4,17E+06
grid200	4,37E+06	1,85E+11	4,16E+05	5,84E+06
grid200_1	4,36E+06	2,26E+11	4,59E+05	6,02E+06

Collected stats midmoment Mz				mean
method	mean value	variance	Stnd dev	maximum
FFT1000	-2,22E+07	5,90E+15	7,67E+07	2,04E+08
FFT500	-2,20E+07	5,69E+15	7,54E+07	2,08E+08
EAP75	-2,21E+07	5,56E+15	7,45E+07	2,12E+08
EAP100	-2,19E+07	5,68E+15	7,53E+07	1,99E+08
EAP200	-2,21E+07	5,51E+15	7,40E+07	1,95E+08
FFTrf75	-2,20E+07	5,60E+15	7,47E+07	1,92E+08
FFTrf100	-2,19E+07	5,83E+15	7,63E+07	1,96E+08
FFTrf200	-2,21E+07	5,78E+15	7,60E+07	2,12E+08
FFTrf1000	-2,23E+07	6,00E+15	7,73E+07	2,09E+08
FFTrfa75	-2,20E+07	5,58E+15	7,39E+07	1,91E+08
FFTrfa100	-2,20E+07	5,42E+15	7,33E+07	1,92E+08
FFTrfa200	-2,23E+07	6,11E+15	7,77E+07	2,07E+08
FFTrfa1000	-2,20E+07	5,71E+15	7,54E+07	2,05E+08
grid200	-1,31E+07	6,33E+15	7,88E+07	1,97E+08
grid200_1	-1,31E+07	6,95E+15	8,27E+07	2,07E+08

A.2.2 Statistics for all time histories ordered for each method.

The spreadsheets for these results are very extensive, and are given as digital attachments to the report.